CHEMICAL REVIEWS

REVIEW

pubs.acs.org/CR

Quantum Monte Carlo and Related Approaches

Brian M. Austin,[†,§] Dmitry Yu. Zubarev,[†] and William A. Lester, Jr.[*,†,‡]

[†]Kenneth S. Pitzer Center for Theoretical Chemistry, Department of Chemistry, University of California at Berkeley, Berkeley, California 94720, United States

[‡]Chemical Sciences Division, Lawrence Berkeley National Laboratory, Berkeley, California 94720, United States

CONTENTS

1. INTRODUCTION

As the name implies, Monte Carlo (MC) methods employ random numbers to solve problems. The range of problems that may be treated by MC is substantial; these include simulation of physical processes, evaluation of multidimensional integrals, solution of integral and linear operator equations, and applications in statistical mechanics. All of these functions of MC can be applied to the treatment of problems arising in quantum mechanics, and the intersection of MC methods and quantum mechanics is generally referred to as quantum Monte Carlo (QMC).[1]

QMC methods have several advantages:

- QMC methods are among the most accurate tools for studying molecular quantum mechanics and include thorough treament of static and dynamic correlation effects. They can provide properties of exact solutions to Schrödinger's equation for Bose ground states. The conventional "fixed-node" approach to fermion systems typically provides high-quality results, whereas other QMC variants can produce exact results for fermions, albeit with exponential scaling computational cost.

Special Issue: 2012 Quantum Chemistry

Received: May 4, 2011
Published: December 23, 2011

- The diffusion Monte Carlo (DMC) variant of QMC has substantially reduced basis set truncation and basis set superposition errors relative to other ab initio methods. For bosonic systems, DMC eliminates basis set errors entirely, whereas for fermions, these errors are finite and manifested indirectly owing to the fixed-node constraint.
- QMC is intrinsically parallel, allowing QMC codes to take advantage of the largest supercomputers with little modification.
- The compute time for each step of a QMC calculation increases roughly as N^3, where N is a measure of system size (i.e., the number of particles of the system). Recent developments have achieved linear scaling in certain cases.
- Computer memory requirements are small and grow modestly with system size.
- Computer codes for QMC are significantly simpler and smaller than those of basis set molecular quantum mechanics computer programs.
- Any Monte Carlo calculation can be improved to achieve whatever degree of statistical precision is needed. The random error of QMC calculations decreases in proportion to the square root of the computational time. This enables one to estimate the compute time needed for performing a calculation with a prescribed error bar.

Expansion and perturbative approaches, such as Hartree−Fock (HF), configuration interaction (CI), many-body perturbation theory (MBPT), and coupled cluster (CC) approaches, dominate the field of molecular quantum mechanics. Methodological improvements and increases in computational resources allow ever-larger systems to be treated with higher levels of accuracy. However, the accuracy of these methods is determined by the one-particle (basis set) and the many-particle (determinants or configuration state functions) expansions used. Because the latter are typically slowly convergent in an orbital representation, computational cost and storage demands can grow rapidly with expansion length and limit the size of systems that can be treated to high accuracy. Methods based on density functional theory (DFT) are not as strongly limited by size considerations but have other challenges.

The QMC method is not constrained by considerations of basis set and many-particle expansions. It is a powerful method capable of high accuracy and is readily adapted to parallel computers. The facile use of highly parallel computer systems sets QMC apart from other other quantum chemical methods. It has been applied to molecular systems containing over 300 electrons and, with the imposition of translational symmetry, to condensed matter systems with over 1000 electrons. The precision of QMC is determined by how accurately the exact wave function can be approximated, as shall be described below. Much has been achieved with the QMC method in the computation of energies and selected other properties for atoms and molecules.

The first published description of quantum Monte Carlo is attributed to E. Fermi in a classic paper by Metropolis and Ulam.[2] Some years later, Kalos[3] proposed Green's function quantum Monte Carlo, which was applied to the calculation of the ground state of three- and four-body nuclei. In retrospect, this paper was indicative of the versatility of QMC for studies of nuclear, condensed matter, and atomic and molecular systems. It remained for Anderson[4] to make the first significant foray into atomic and molecular systems in the mid-1970s. These classic papers introduced the fixed-node approximation, which has served as a bellwether for the DMC variant of QMC as described below.

1.1. Scope of the Review

The focus in this review is the use of QMC to solve the electronic Schrödinger equation for atoms and molecules, an area that historically has been labeled ab initio quantum chemistry. Earlier reviews[1,5−16] complement the coverage provided in this contribution. Several computational physics texts also contain chapters about QMC.[17−19]

This review attempts to achieve a reasonable balance between the level of technical details in the presentation of formal aspects of QMC methodology pertinent to different approaches and broader coverage of significance and potential of QMC studies in resolving contemporary chemical problems. The most common approaches to QMC are described in section 2. These include variational MC (VMC), DMC, auxiliary field QMC, reptation MC, and a handful of other selected approaches. The preceding methods are distinct from finite-temperature methods such as path integral MC (PIMC), which are reviewed in refs 20 and 21. Section 3 covers critical aspects of QMC calculations, such as construction and improvement of trial wave functions. Some topics pertinent to computational efficiency are discussed in sections 4 and 5. A range of problems addressed in recent QMC investigations of electronic structure of atoms and molecules and the main challenges to the QMC approach are reviewed in section 6.

Certain domains of QMC application are beyond the scope of the present contribution. These include studies of rotational and vibrational states, including spectroscopy of ultracold clusters,[22−34] and some condensed matter problems,[14,20,35−45] although many of the methods applied to the latter are directly applicable to atoms and molecules. There have been significant advances made in the application of QMC to the nuclear Schrödinger equation. This area will also not be discussed in this review. The interested reader is referred, for example, to refs 46−48.

2. QUANTUM MONTE CARLO APPROACHES

In this section, we provide a theoretical background for several established and emerging QMC computational methods. The applicability of MC methods is diverse and spans classical statistical mechanics simulations, operations research, and statistical analysis. Details of common MC techniques such as importance sampling, correlated sampling, and MC optimization are available from multiple sources.[49−59] Here, we summarize the variational (VMC) and diffusion MC (DMC) approaches. Our discussion of alternative QMC techniques focuses on their conceptual foundations and their advantages and challenges relative to VMC and DMC.

2.1. Variational Monte Carlo

The VMC method uses MC integration[60] to compute molecular properties from a trial wave function. In the jargon of QMC, a trial wave function is an approximation to the "true" wave function that solves the Schrödinger equation exactly. One may estimate the energy of a trial wave function by MC integration and obtain a more accurate wave function by varying the parameters of the trial function to minimize the energy estimate. The following discussion shows how the MC integration techniques may be adapted to the evaluation of expectation values and matrix elements and describes methods and criteria for optimizing wave functions.

The variational energy of an arbitrary wave function is given by the expectation value of the Hamiltonian: $E = \langle\Psi|\hat{H}|\Psi\rangle/\langle\Psi|\Psi\rangle$. To evaluate the energy by VMC, the Hamiltonian and overlap integrals that appear in the expectation value are rewritten in the

form of eq 1.

$$\int f(\mathbf{X})\rho(\mathbf{X})\,\mathrm{d}\mathbf{X} = \lim_{K\to\infty}\frac{1}{K}\sum_{k:\mathbf{X}_k\in\rho}^{K} f(\mathbf{X}_k) \tag{1}$$

Here, k enumerates points sampled from the probability density function (PDF) $\rho(\mathbf{X})$. A natural choice for the PDF is the normalized square of the trial wave function: $\rho(\mathbf{X}) = {\Psi_\mathrm{T}}^2(\mathbf{X})/\int {\Psi_\mathrm{T}}^2(\mathbf{Y})\,\mathrm{d}\mathbf{Y}$. This density may be sampled using the Metropolis method.[60] The energy can then be computed as follows,

$$E = \int \rho(\mathbf{X})\frac{\hat{H}\Psi_\mathrm{T}(\mathbf{X})}{\Psi_\mathrm{T}(\mathbf{X})}\,\mathrm{d}\mathbf{X} = \frac{1}{K}\sum_{k:\mathbf{X}_k\in{\Psi_\mathrm{T}}^2}^{K} E_\mathrm{L}(\mathbf{X}_k) \tag{2}$$

where the "local energy" of Ψ at $\mathbf{X}$ is defined by $E_\mathrm{L}(\mathbf{X}_k) = \hat{H}\Psi(\mathbf{X})/\Psi(\mathbf{X})$. The simple form of eq 2 is due to the selection of ${\Psi_\mathrm{T}}^2/\int {\Psi_\mathrm{T}}^2$ as the PDF. Because Ψ_T is an approximate eigenfunction of the Hamiltonian, $H\Psi_\mathrm{T} \approx E\Psi_\mathrm{T}$, the variance of the local energy approaches zero as Ψ_T approaches the exact eigenfunction. The relatively small variance of the local energy allows VMC to estimate the energy much more efficiently than other properties whose operators do not commute with the Hamiltonian.

The VMC method can also be used to evaluate general matrix elements of the form $A_{ij} = \langle\Psi_i|\hat{\mathcal{O}}|\Psi_j\rangle$.[61] This integral may be rewritten in the form of eq 1.

$$\begin{aligned}\langle\Psi_i|\hat{A}|\Psi_j\rangle &= \int \kappa(\mathbf{X})\frac{\Psi_i(\mathbf{X})\hat{A}\Psi_j(\mathbf{X})}{\kappa(\mathbf{X})}\,\mathrm{d}\mathbf{X}\\ &= \frac{1}{K}\sum_{k:\mathbf{X}_k\in\kappa}^{K}\frac{\Psi_i(\mathbf{X}_k)\Psi_j(\mathbf{X}_k)}{\rho(\mathbf{X}_k)}\frac{\hat{A}\Psi_j(\mathbf{X}_k)}{\Psi_j(\mathbf{X}_k)}\end{aligned} \tag{3}$$

Coordinates are sampled from the PDF, κ, and the matrix element is evaluated using the average indicated in eq 3. Several further complications arise when computing off-diagonal matrix elements. First, there is no obvious choice for κ when computing off-diagonal matrix elements. Averages of ${\Psi_i}^2$ and ${\Psi_j}^2$ are sometimes used[62] so that the densities of both wave functions are sampled, but this choice is somewhat arbitrary. Second, there is little reason to expect the summand of eq 3 to have a particularly small variance, so accurate evaluations of matrix elements are more computationally demanding than energies.[63]

2.2. Fixed-Node Diffusion Monte Carlo (FNDMC)

Although considerable research focuses on the development of high-quality trial functions, the accuracy of the VMC method will always be limited by the flexibility and form of the trial wave function. Highly accurate solutions to the Schrödinger equation can be computed by DMC, which uses MC methods for both solving the Schrödinger equation and integrating expectation values. DMC is rooted in the time-dependent Schrödinger equation and its solutions,

$$\frac{\mathrm{d}}{\mathrm{d}t}\Phi(\mathbf{X},t) = -iH\Phi(\mathbf{X},t) \tag{4a}$$

$$\Phi(\mathbf{X},t) = \mathrm{e}^{-itH}\Phi(\mathbf{X},t=0) \tag{4b}$$

By expanding the wave function $\Phi(\mathbf{X},t)$ in eigenfunctions of H and shifting the potential by the ground-state energy, one obtains solutions that converge to the ground state when the imaginary time, $\tau = it$, becomes large:

$$\begin{aligned}\Phi(\mathbf{X},\tau) &= \mathrm{e}^{-\tau(H-E_0)}\left(\sum_j c_j\Psi_j(\mathbf{X})\right)\\ &= \sum_j c_j\,\mathrm{e}^{-\tau(E_j-E_0)}\Psi_j(\mathbf{X})\\ \lim_{\tau\to\infty}\Phi(\mathbf{X},\tau) &= c_0\Psi_0(\mathbf{X})\end{aligned} \tag{5}$$

The DMC method extracts the ground-state wave function by propagating the Schrödinger equation in imaginary time. This is accomplished by exploiting an isomorphism between the kinetic energy term in the Hamiltonian and a classical diffusion equation; the latter can be simulated by a random walk. A second isomorphism exists between the potential energy and a spatially inhomogeneous first-order rate equation that can be simulated by a branching process.

$$\frac{d}{d\tau}\Phi(\mathbf{X},\tau) = \left(\underbrace{\frac{1}{2}\nabla^2}_{\text{Diffusion}} \underbrace{-(V(\mathbf{X})-E_0)}_{\text{Branching}}\right)\Phi(\mathbf{X},\tau). \tag{6}$$

2.2.1. Diffusion. The connection between diffusion and random walks was established by Einstein in a study of Brownian motion.[64] Suppose a collection of points, $\mathbf{X}$ ("walkers"), is initially sampled from $\rho(\mathbf{X}, \tau = 0)$ and that, after a short time, each walker takes an independent random step, η, sampled from a $3N$-dimensional Gaussian distribution with standard deviation $(2D\tau)^{1/2}$:

$$g(\eta,\tau) = [4\pi D\tau]^{-3N/2}\exp(-\eta^2/4D\tau) \tag{7}$$

The updated density function will then be

$$\rho(\mathbf{X},\tau) = \int \rho(\mathbf{X}-\eta,\tau)g(\eta,\tau)\,\mathrm{d}\eta \tag{8}$$

The property that eq 7 solves the diffusion equation for a point source with diffusion constant of D can be used to show that $\mathrm{d}\rho/\mathrm{d}\tau = D\nabla^2\rho$. This result indicates that one may start from any initial density function and simulate its solution to the diffusion equation using an ensemble of walkers taking random steps.

2.2.2. Branching. Neglecting the diffusion term in eq 6 leads to an equation that is easily solved,

$$\frac{\mathrm{d}}{\mathrm{d}\tau}\Phi(\mathbf{X},\tau) = -(V(\mathbf{X})-E_0)\Phi(\mathbf{X},\tau) \tag{9a}$$

$$\Phi(\mathbf{X},\tau) = \exp[-(V(\mathbf{X})-E_0)\tau]\Phi(\mathbf{X},\tau) \tag{9b}$$

The solutions to this equation manifest in the MC algorithm by associating a weight, w_k, with each walker. Initially, each walker has unit weight (i.e., $w_k = 1$), and its weight is updated at each step according to $w_k(\tau+\Delta\tau) = w_k(\tau)\exp[-(\mathrm{V}(\mathbf{X})-E_0)\Delta\tau)]$. The weights of a collection of walkers tend to diverge,[65] so only a small number of walkers contribute to any MC average.[65] For this reason, it is computationally advantageous to replace weights by a stochastic birth/death process in which walkers with weights > 1 create offspring at the same position with a probability of $w_k - 1$ and walkers with weights < 1 will die with probability $1 - w_k$.

2.2.3. Short-Time Approximation. The random walk and branching processes provide exact solutions to their respective differential equations, so it is tempting to combine the two by

dx.doi.org/10.1021/cr2001564 |Chem. Rev. 2012, 112, 263–288

advancing one step according to the diffusion equation, then another by the branching equation. DMC does exactly that. The Trotter−Suzuki formula (eq 10) shows that, even if the alternating steps are performed symmetrically, separating the diffusion and branching process creates an $\mathcal{O}(\tau^3)$ error known as the time-step bias.

$$\exp^{-(T+V)\tau} = \exp\left[-\frac{1}{2}V\tau\right]\exp[-T\tau]\exp\left[-\frac{1}{2}V\tau\right] + \mathcal{O}(\tau^3) \quad (10)$$

The large-τ limit is instead reached by iterative application of short-time solutions:

$$\begin{aligned}\Phi(x,\tau) &= \exp(-(T+V)\tau)\\ &= \lim_{n\to\infty}\prod_n \exp\left(-(T+V)\frac{\tau}{n}\right)\\ &= \lim_{n\to\infty}\prod_n \exp\left(-\frac{V}{2}\frac{\tau}{n}\right)\exp\left(-T\frac{\tau}{n}\right)\exp\left(-\frac{V}{2}\frac{\tau}{n}\right)\end{aligned} \quad (11)$$

To remove the time-step bias, a series of DMC calculations with progressively smaller time steps may then be used to extrapolate to the zero time-step result. The requirement of a short time step makes DMC calculations significantly more costly than VMC, and several clever modifications to the random walk algorithm have been introduced to minimize time-step error.[66,67]

2.2.4. Trial Functions and DMC. DMC calculations use a trial function to steer the importance sampling[68] of the mixed density $\rho = \Phi\Psi_T$ instead of $|\Phi|$ or Φ^2. The mixed density evolves according to a transformation of the time-dependent Schrödinger equation that can be derived by multiplying eq 6 by Ψ_T:

$$\frac{d}{d\tau}\rho(\mathbf{X},\tau) = \underbrace{\frac{1}{2}\nabla^2\rho}_{\text{Diffusion}} - \underbrace{\frac{1}{2}\nabla\cdot\left(\frac{2\nabla\Psi_T(\mathbf{X})}{\Psi_T(\mathbf{X})}\rho\right)}_{\text{Drift}} - \underbrace{(E_L(\mathbf{X})-E_0)\rho}_{\text{Branching}}. \quad (12)$$

The introduction of the trial function also modifies the branching term so that the branching rate depends on the local energy instead of the potential. This leads to a suppression of the branching process because the local energy of a good trial function is nearly constant and is generally a good approximation to the exact energy, E_0. In particular, uncontrolled branching at points where the Coulomb potential is singular can be curtailed by choosing a trial function that satisfies the cusp conditions.[69] As the variance of the local energy of the trial function decreases, the branching factor $\exp[-(E_L(\mathbf{X})-E_0)\Delta\tau]$ approaches a constant value. In this limit, the diffusion and drift operators commute. Time-step errors can therefore be reduced by improved trial functions and eliminated by the exact one.

2.2.5. Fixed-Node Approximation. The trial function can also be used to define the fixed-node approximation (FNA), which constrains the DMC solution to have the nodes of Ψ_T. The FNA is enforced during the random walk by forbidding a walker from taking a step that generates a trial function sign change. This condition is implemented by killing the walker. The FNA is essential for efficient application of DMC to fermions because imposing the nodes of an antisymmetric trial function on the solution of the (imaginary) time-dependent Schrödinger equation forces the DMC solution to be antisymmetric as well. Without the fixed-node constraint, DMC calculations would converge to the ground state without symmetry restriction, which is a bosonic state. With the FNA, the stationary states of eq 6 are exact solutions of the Schrödinger equation subject to the approximate fixed-node boundary condition. The nodes of the trial function solely determine the accuracy of FNDMC. Away from nodes, where the trial function is nonzero, the variance of the local energy determines the efficiency of the calculation. More specifically, when the trial function has the Slater−Jastrow form: $\Psi_T = \Psi_A e^U$, the nodes are given solely by Ψ_A because the Jastrow function is positive everywhere. For a given Ψ_A, the FNDMC energy will be the same for all forms of U. The correlation function e^U is important for reducing the variance of the local energy and the number of points needed to reduce the statistical error to an acceptable level.

The nodes of the exact wave function are known for only a few simple systems, so the fixed-node constraint is an approximation. Unlike time-step error, it is not possible to correct for fixed-node error by extrapolation. The error introduced by the FN constraint is the only uncontrolled approximation in the FNDMC method. Fortunately, the FNA is quite good, even when modest trial functions are used. For 55 molecules in the "Gaussian-1 set",[70] atomization energies computed using FNDMC were typically within 3 kcal/mol (average absolute deviation) of experimental reference data.[71]

The centrality of the FNA has spawned considerable research into improvement of the approach. The strategies for obtaining better nodes are numerous. The conventional approach is to select a trial wave function believed to have better nodes (see section 3). Single configuration wave functions have been constructed from canonical HF orbitals, Kohn−Sham orbitals from DFT, and natural orbitals from post-HF methods. Note that multiconfiguration wave functions do not necessarily have better nodes than single configuration wave functions unless their coefficients are reoptimized in the presence of a correlation function.[72−76] More success has been found with alternative wave function forms that include correlation more directly than sums of Slater determinants. These include antisymmetrized geminal power functions,[77,78] valence-bond[79] and Pfaffian[80] forms, and backflow transformed determinants.[81] Only recently have systematic improvements to the nodes been made possible by optimization of Ψ_A in the presence of a correlation function,[82] an idea put forth earlier by Reynolds et al.[83]

A different approach to the node problem is to develop a mathematical or physical understanding of the differences between good and bad nodal surfaces so that trial functions with better nodal surfaces can be constructed. Relatively little is known about wave function nodes.[73] One often mentioned exception is the tiling theorem:[84] the nodal pockets of the Fermi ground state are the same within permutational symmetry. Plotting and comparing nodes may provide physical insight into some features of the exact nodes.[85,86] Plots of a Pfaffian wave function have revealed tunnels between nodal pockets that are not present in HF wave functions,[80] but the high dimensionality and complicated structure of the nodes make it difficult, in general, to translate these observations into an improved ansatz. A mathematical analysis of the FNA has been presented by Cances et al.[87]

A few alternatives to the FN constraint are available within QMC. The released node method starts from a FNDMC calculation.[35,88] When the FN constraint is relaxed (released node QMC) an estimate of the exact ground-state energy may be

obtained by incorporating a factor of −1 for each walker that crosses the nodal surface:

$$E = \frac{\sum_k s_k w_k E_L(\mathbf{X}_k)}{\sum_k s_k w_k}; s_k = \mathrm{sgn}[\Psi_T(\mathbf{X}_k(\tau))\Psi_T(\mathbf{X}_k(0))] \quad (13)$$

As the number of walkers that cross nodes increases, so does the cancellation between positive and negative contributions to the averages, leading to rapid growth of the variance as the denominator approaches zero. Furthermore, the rate of this degeneration increases with the difference in energy between the Fermi and Bose ground states, which may be unusably fast for molecules of substantial size.

Other alternatives to the FN approach include the A-function method.[89−91] The method builds nodal surfaces as a sum of Gaussian functions centered on DMC walkers.

Green's function Monte Carlo (GFMC)[3,54,92] relies on the standard resolvent operator of Schrödinger equation,

$$\hat{P}(\hat{H}) = \frac{1}{1 + (\hat{H} - E_R)\delta\tau} \quad (14)$$

instead of the imaginary-time evolution operator,

$$\hat{P}(\hat{H}) = e^{-(\hat{H} - E_R)\delta\tau} \quad (15)$$

GFMC does not have time-step error, but its computational time is higher than that of DMC. This makes GFMC a less common choice for treatment of molecular or atomic electronic structure problems.

Another method is Fermion Monte Carlo (FMC)[93,94] (also known by some authors as exact QMC[95−97]), for which nodes of the trial function play no special role. In this approach, antisymmetry is maintained by careful cancellation of positive and negative walkers. Though FMC methods have achieved remarkable accuracy for small systems such as H_3^+[98] and H_3,[99] FMC methods that can be practically used for larger systems are under development.

2.3. Self-Healing Diffusion Monte Carlo

The improvement of FNDMC energies is possible only by improving the nodal surface of the trial wave function. The quality of VMC optimization is limited by the fact that the VMC sampling occurs far from nodes. Self-healing DMC (SHDMC) optimizes nodal surfaces directly[100−102] by locally removing kinks in the FN ground-state wave function. These kinks are manifestations of discontinuities in the gradient at the nodal surface of the trial wave function. In SHDMC, an improved nodal surface is obtained by sampling walkers from a DMC ensemble and convolving the walker density with a smoothing function to generate a new antisymmetric wave function.

SHDMC is applicable to both ground[101] and excited[102] states. It was shown to converge systematically to a high-accuracy CI solution for the ground state of oxygen atom and yielded a binding energy of N_2 with near-chemical accuracy. The computational cost of the SHDMC approach scales linearly with the number of degrees of freedom of the nodes, and molecules as large as C_{20} have been studied.[100] Its accuracy depends only on the size of the available statistics and the flexibility of the form of trial wave function.

2.4. Auxiliary Field Quantum Monte Carlo

The FN constraint is avoided entirely in the auxiliary field QMC (AFQMC) method[103−105] where random walks are performed in the space of Slater determinants. The sign problem manifests differently in AFQMC, and analogous constraints must be used. Like other QMC methods, AFQMC uses an imaginary-time propagator to project out contributions of excited states in the trial wave function to obtain the ground-state solution. Unlike FNDMC, the random walk occurs in a space of nonorthogonal Slater determinants rather than in the position space of n-particle configurations so that the antisymmetry of each walker (and the ensemble of walkers) is ensured without special treatment. To propagate the Slater determinants in imaginary time, the Hubbard−Stratonovich transformation is used to recast the two-body term in the Hamiltonian as a linear combination of fluctuating one-body auxiliary fields.[106] This can be done using any single-particle basis set, including plane waves and Gaussian-type functions.[106,107] A severe problem emerges, however, in the treatment of two-body interactions because the one-body operators are, in general, complex. For large projection times, the phase of each orbital becomes random and the AFQMC wave function is dominated by noise. This phase problem is analogous to the fermion sign problem. The phaseless AFQMC approach[108] addresses this issue by confining the random walk based on overlap of each walker with a trial wave function. The ground-state energy in phaseless AFQMC is nonvariational. In addition, the method is more sensitive to basis set truncation than DMC. The phaseless AFQMC method has been successfully applied to the energetics of selected atomic, molecular, and hydrogen-bounded systems.[106−109]

2.5. Reptation Quantum Monte Carlo

Reptation quantum Monte Carlo (RQMC) is directed at computing unbiased expectation values of operators that do not commute with Hamiltonian. This task is challenging in the DMC framework because the mixed estimators, $\langle\Phi|\hat{\mathcal{O}}|\Psi_T\rangle$, that are most readily obtained include biases introduced by the trial function. Although the forward walking technique[110] can be used to eliminate this bias, it is subject to substantially larger statistical fluctuations than the mixed estimator.[111] The RQMC technique was devised to evaluate propertis of the "pure" distribution, Φ^2, with reduced variance.

RQMC can be viewed as a modification of a pure diffusion QMC method insofar as the imaginary-time dynamics of the quantum system are mapped onto a classical diffusion process.[112] However, the basic variable of RQMC is a "reptile" that corresponds to the path of a DMC-like random walk. This allows the method to sample the product of a joint probability distribution for the reptile and a Boltzman factor involving the discretized integral of the local energy along the length of the reptile.

Expectation values are computed by averaging over reptile random walks.[113] In the FN variant of RQMC approach, estimates of the exact energy are obtained from the first and last configurations of the reptiles. The middle configurations are used to estimate expectation values of operators that do not commute with the Hamiltonian.

A number of variations of the original RQMC method have been developed.[114,115] Metropolis−Hastings RQMC corrects for irreversibility problems that were not properly addressed in the original RQMC but fails to meet the assumed criterion of microreversibility. The resulting accumulation of the time-step bias is resolved in "no-compromise" RQMC, which relaxes the microreversibility requirement and leads to stabilization of the middle configurations of reptiles.[114] Further development of "head−tail adjusted" RQMC addresses the issue of low practical

dx.doi.org/10.1021/cr2001564 |Chem. Rev. 2012, 112, 263–288

efficiency of no-compromize RQMC, which suffered from a high rejection ratio during the random walk and a correspondingly large accumulation of error.

2.6. Full CI Quantum Monte Carlo

The recently developed full configuration interation (FCI)-QMC method uses an MC approach to efficiently obtain an FCI wave function.[116−118] In FCI-QMC, the random walk occurs in the space of the Slater determinants that form the FCI expansion. Unlike DMC, there is no diffusion associated with the random walk. The simulation ensemble consists of signed walkers, each associated with a Slater determinant. The ensemble of walkers evolves according to a set of population dynamics rules derived from the imaginary-time evolution propagator. A walker can die or be cloned with a certain probability and it can spawn a new walker at a connected Slater determinant. Pairs of walkers of opposite sign on the same determinant are annihilated. The CI amplitude on a determinant is then defined to be proportional to the signed sum of walkers of the determinant. The stochastic description of a FCI wave function eliminates the requirement for concurrent storage of all amplitudes. The entire space of symmetry-allowed determinants is accessible for the random walk, so that the simulation ultimately samples the FCI wave function. Evolution in the space of Slater determinants prevents convergence to a bosonic solution but does not eliminate the sign problem, which reappears in the inability to a priori predict signs of CI coefficients. The computational complexity of FCI-QMC scales similarly to conventional FCI, but smaller scaling constants make larger FCI spaces computationally feasible. The FCI-QMC approach has been successfully used to obtain total energies of small molecules,[118] including some systems too challenging for conventional FCI, and ionization potentials of atoms from Li to Mg.[116]

2.7. Time-Dependent Quantum Monte Carlo

The previously described QMC methods rely on random walks in the space of electron configurations. Methods that utilize the time-dependent Schrödinger equation with imaginary time do not yield real-time dynamics of electrons in physical space. In time-dependent QMC (TDQMC), each physical particle is a walker guided by an individual de Broglie−Bohm pilot-wave[119−123] TDQMC can be seen as a set of coupled time-dependent Schrödinger equations for the guiding waves in physical space and a de Broglie−Bohm guiding equation without quantum potentials for the walkers in physical space. The density of walkers represents density of the corresponding physical particles, and the intrinsic statistical nature of quantum objects is due to guiding waves. Interactions between electrons are accounted for using explicit Coulomb potentials and pseudopotentials to describe nonlocal correlation effects. One of the advantages of TDQMC is its insensitivity to the sign problem, which is due to correspondence between walker distribution and quantum probability density. TDQMC is capable of describing real-time evolution of quantum systems including their interaction with external fields at a fully correlated level.

3. TRIAL ELECTRONIC WAVE FUNCTIONS

Although QMC methods are capable of computing molecular properties accurately, most do not yield a wave function per se but instead sample the many-electron density. Trial wave functions that are used to guide these calculations have a strong influence on the computational efficiency of the calculation and a subtle influence on accuracy. It is therefore desirable to have an accurate analytical expression for the wave function. Although the QMC energy is determined by nodes of the wave function, neither the Metropolis algorithm nor MC integration depends on the form of Ψ_T. Even the most elaborate trial wave functions can be explored at low cost without modifying the VMC algorithm. The accuracy of a flexible trial function cannot be realized without optimizing its parameters. This section presents several common forms of the electronic wave function and describes a few of the approaches developed to optimize the trial function.

Typically QMC calculations are carried out in the FNA using a Slater−Jastrow (SJ) wave function, which is written as a product of an antisymmetric function, Ψ_A, and an exponentiated Jastrow function, U: $\Psi_{SJ} = \Psi_A e^U$. The antisymmetric function describes the fundamental properties of the wave function including permutational or spin symmetry. The symmetric Jastrow function depends explicitly on interelectronic distance and provides a compact description of short-range, dynamically correlated electronic motion.

3.1. Antisymmetric Wave Functions

Most basis set ab initio methods build many-electron wave functions from atomic orbitals (AOs) or molecular orbitals (MOs). The simplest many-electron wave functions constructed from MOs are obtained from HF theory. Multiconfiguration wave functions are more general than HF wave functions and may approach the exact solution in certain limits.

Historically, MO methods have dominated trial-function construction because these functions are readily obtained from widely distributed computer codes. Recently, however, some QMC practitioners have renewed interest in a broader variety of wave functions including valence bond (VB) functions,[79] pairing wave functions, such as the antisymmetrized geminal power (AGP),[77,78] Pfaffian, and perfect pairing forms.[80] All of these wave function types can be modified by backflow transformations.[124]

3.1.1. Orbital Parameterization. A generic spin−orbital is a function of electron spatial coordinates, $\mathbf{r} = (x, y, z)$, and spin coordinate, ω. The combined space/spin coordinate is denoted by $\mathbf{x} = (\mathbf{r}, \omega)$.

$$\psi(\mathbf{x}) = \psi^{\alpha}(\mathbf{r})\alpha(\omega) + \psi^{\beta}(\mathbf{r})\beta(\omega) \tag{16}$$

The spin functions, $\alpha(\omega)$ and $\beta(\omega)$, are eigenfunctions of the square of the one-electron spin operator ($\hat{s}^2$) and the projection of $\hat{s}$ on the z-axis ($\hat{s}_z$). Spin orbitals are often constrained to have only α- or β-character and a common convention is to use unbarred symbols to indicate α-spin orbitals (i.e., $\psi = \psi^{\alpha}\alpha$) and barred symbols for the β-spin orbitals (i.e., $\overline{\psi} = \psi^{\beta}\beta$). The spatial orbitals are typically (but not necessarily) expanded in a basis set. Basis sets can be chosen somewhat arbitrarily, but the quality of the possible choices can be judged by considering completeness of the basis set and how quickly the basis converges to eigenfunctions of the Hamiltonian. The most commonly used basis sets include plane waves, Slater-type orbitals (STO), Gaussian-type orbitals (GTO), and numerical orbitals.

The plane wave basis is not as well suited for the molecular Hamiltonian as GTOs and STOs. The electron−nucleus cusp conditions cannot be satisfied for any finite-size plane wave basis, although this problem can be avoided by using effective core potentials. The periodicity of plane wave basis functions makes this basis preferable for solids compared to isolated molecules.[125]

Several desirable wave function properties are obtained with the use of STOs.[126] The long-range tail of each function has an exponential dependence, making it easier to match the correct

asymptotic behavior of the electron density. The electron−nucleus cusp condition is readily satisfied by STO functions.

Many of the integrals needed to evaluate molecular energies cannot be evaluated analytically with STOs, which led to the use of GTOs owing to ease of integration.[127] Several advantages of STOs are not retained with GTOs. The radial component of the GTO has a zero derivative at the origin so a single GTO cannot satisfy the electron−nucleus cusp condition.[128] In addition, GTO basis sets are not complete. Nevertheless, carefully tuned linear combinations of GTO's with assorted exponents (contracted GTO's) have been developed to give adequate descriptions of the molecular Hamiltonian,[127] and advantageous trade-offs between expedience and accuracy make contracted GTOs the dominant basis sets used in quantum chemistry. Recently, mixed Gauss−Slater basis sets have been proposed for calculations with pseudopotentials.[129]

In addition to basis set expansions, there are various numerical methods for parametrizing orbitals including numerical basis sets of the form $\phi(\mathbf{r}) = Y_{lm}(\mathbf{r})f(r)$, in which the radial function, $f(r)$ does not have an analytical form but is evaluated by a spline procedure.[130] Numerical orbitals may be more flexible than STO or GTO basis sets, but their use is more computationally demanding. Wavelet representations of orbitals[131] are exceptionally flexible as well and have an intriguing multiresolution property: wavelet algorithms adaptively increase the flexibility of the orbital in regions where the molecular energy depends sensitively on the precision of the orbital and use coarser descriptions where precision is less essential.

3.1.2. Hartree−Fock Wave Functions. One can construct a simple many-electron wave function by forming the antisymmetrized product of orbitals. This is conveniently evaluated using the determinant of the Slater matrix, whose elements are the values of each orbital (in rows) evaluated at the coordinates of each electron (in columns). Linear combinations of Slater determinants can be used to construct configuration state functions (CSFs) that satisfy the total spin constraints (plus any additional symmetry-related requirements).

HF wave functions are obtained by minimizing the energy of a single CSF with respect to variations of the spatial orbitals. The HF energy is not exact because the HF wave function does not account for electron correlation in singlet wave functions; for triplet wave functions, correlation is included through the antisymmetrizer. The difference between the HF energy and the exact energy is known as the correlation energy, $E_{corr} = E_{HF} - E_{exact}$. The correlation energy is typically a small percentage of the total energy,[132] but this relatively small error is often larger than the energy differences that account for a large number of chemical phenomenon. The need for chemical accuracy emphasizes the importance of exploring more elaborate wave functions and the HF wave function provides a starting point for many of these methods.

3.1.3. Configuration Interaction Wave Functions. The simplest approach to evaluating the correlation energy is to increase the number of configurations that contribute to the wave function. Once a reference configuration has been obtained from a HF calculation, a set of related substituted determinants may be identified. The substituted determinants are related to the reference by replacing the orbitals from the occupied space with orbitals from the unoccupied space. The configuration interaction (CI) method then minimizes the variational energy of a wave function formed from a linear combination of determinants (or, equivalently, CSFs) with respect to the CI coefficients. In principle, CI calculations can provide exact results if the single-particle basis is complete and the full set of CSFs is used in the CI expansion (full-CI). The second condition is exceptionally demanding. The number of determinants included in a calculation with N electrons and K spatial basis functions is $((2K)!)/(N!(2K - N)!)$, making full-CI calculations prohibitively expensive for all but the smallest molecules. Truncated CI calculations in which a small number of orbitals are substituted into the reference configuration are feasible, and a hierarchy of CI methods is formed by adding increasingly substituted configurations to the CI expansion. CI with single substitutions (CIS) is commonly used to estimate excitation energies, but truncated CI does not provide a size-consistent treatment of the correlation energy. In practice, CI calculations that include up to four substitutions (CISDTQ) are nearly size-consistent.[133] The MCSCF (multiconfiguration self-consistent field) method is akin to truncated CI in the sense that the MCSCF also expresses the wave function as a linear combination of CSFs, but it differs from CI in that the orbitals are optimized simultaneously with the CI coefficients.[134]

Among MO based theories, dynamic correlation is better described by perturbation theory or coupled cluster approaches,[135] which are both accurate and computationally affordable, at least for small- to medium-sized molecules. Despite their prevalence in quantum chemistry, these methods will not be described here because the number of determinants required to evaluate their wave functions is presently too large to be used as QMC trial functions.

3.1.4. Valence-Bond Wave Functions. Valence-bond theory provides another class of wave functions.[136,137] General VB wave functions are linear combinations of "structures" with the form

$$\Omega_{S,M,k}(\mathbf{X}) = \hat{\mathcal{A}}([\phi_{k,1}(\mathbf{r}_1)...\phi_{k,N}(\mathbf{r}_N)]\Theta_{S,M,k}(\omega_1,...,\omega_n)) \tag{17}$$

Here, $\hat{\mathcal{A}}$ is the antisymmetrizer and $\phi_{k,\nu}$ are the atomic basis functions that participate in the kth structure. The spin function $\Theta_{S,M}$ is constructed to make each structure an eigenfunction of the squared total spin angular momentum operator $\hat{S}^2$, and the projection of the total spin onto the z-axis, $\hat{S}_z$ with quantum numbers S and M. VB theory has many variants that can be classified by their methods of selecting structures for the calculation. A more complete enumeration of VB wave functions can be found in refs 136−138.

3.1.5. Pairing Wave Functions. An alternative approach to improving upon HF wave functions is to include correlations between pairs of electrons more directly by means of two particle "geminal" functions, $G(\mathbf{x}_i, \mathbf{x}_j)$. The antisymmetrized geminal power (AGP), Pfaffian, and perfect pairing wave functions are all examples of pairing wave functions; each can be written as an antisymmetrized product of geminals, $\Psi = \hat{\mathcal{A}}\prod_i G_i(\mathbf{x}_{2i}\mathbf{x}_{2i+1})$ that differ in the form of G.

The singlet AGP wave function[77] for $2N$ electrons shares the same singlet coupled spin geminal for each pair:

$$\begin{aligned} {}^1\Psi_{AGP} &= \hat{\mathcal{A}}\,[G(\mathbf{x}_1,\mathbf{x}_2)G(\mathbf{x}_{2N-1},\mathbf{x}_{2N})] \\ G_{AGP}(\mathbf{x}_i,\mathbf{x}_j) &= g(\mathbf{r}_i,\mathbf{r}_j)[\alpha(\omega_1)\beta(\omega_2) - \alpha(\omega_2)\beta(\omega_1)] \\ g(\mathbf{x}_i,\mathbf{x}_j) &= \sum_{\mu\nu} c_{\mu\nu}\phi_\mu(\mathbf{x}_i)\phi_\nu(\mathbf{x}_j) \end{aligned} \tag{18}$$

The spatial geminals are symmetric with respect to the exchange of particle coordinates and may be expressed as a linear combination of basis functions, ϕ_μ, in which the matrix of coefficients is

dx.doi.org/10.1021/cr2001564 |Chem. Rev. 2012, 112, 263–288

symmetric (i.e., $c_{\mu\nu} = c_{\nu\mu}$). An additional K unpaired electrons may be included in an extended AGP wave function by appending the unpaired orbitals to the geminal product:

$$^{K+1}\Psi_{\mathrm{AGP}} = \hat{\mathcal{A}}\left[G(\mathbf{x}_1,\mathbf{x}_2)G(\mathbf{x}_{2N-1},\mathbf{x}_{2N})\psi_1(\mathbf{x}_{2N+1})\psi_K(\mathbf{x}_{2N+K})\right] \quad (19)$$

The AGP wave function can be efficiently evaluated as the determinant of an $(N + K) \times (N + K)$ determinant.[78,139]

Pfaffian wave functions[80] are distinguished from AGP wave functions by the addition of triplet coupled terms to the spin geminal:

$$\begin{aligned}\Psi_{\mathrm{Pf}} &= \hat{\mathcal{A}}\left[G_{\mathrm{Pf}}(\mathbf{x}_1,\mathbf{x}_2)\ldots G_{\mathrm{Pf}}(\mathbf{x}_{2N-1},\mathbf{x}_{2N})\right]\\ G_{\mathrm{Pf}}(\mathbf{x}_1,\mathbf{x}_2) &= g^{\alpha\beta}(\mathbf{r}_1,\mathbf{r}_2)(\alpha(\omega_1)\beta(\omega_2)\\ &\quad -\beta(\omega_1)\beta(\omega_2))/\sqrt{2} + h^{\alpha\alpha}(\mathbf{r}_1,\mathbf{r}_2)(\alpha(\omega_1)\alpha(\omega_2))\\ &\quad +h^{\beta\beta}(\mathbf{r}_1,\mathbf{r}_2)(\beta(\omega_1)\beta(\omega_2)) \end{aligned} \quad (20)$$

Spatial geminals for the triplet pairs, $h^{\sigma\sigma'}$, can also be expressed as linear combinations of basis functions, but their coefficient matrices must be antisymmetric. Clearly, the Pfaffian form reduces to the AGP wave function when $h^{\alpha\alpha} = h^{\beta\beta} = 0$. Reference 80 provides a thorough description of the Pfaffian wave function and an efficient algorithm for evaluating the Pfaffian of a matrix by first bringing the matrix into a block diagonal form.

3.1.6. Perfect Pairing Wave Functions. In the perfect pairing model, each pair of electrons is described by its own geminal. In contrast, the AGP and Pfaffian functions share the same geminal for all electron pairs. The perfect pairing (PP) geminal has a more constrained form than the previously described wave functions. In each geminal, a pair of "active occupied" orbitals, $\psi_i\psi_{\bar{i}}$, has a corresponding i pair of "active virtual" orbitals, $\psi_{i^*}\psi_{\bar{i}^*}$:

$$\begin{aligned}\Psi_{\mathrm{pp}} &= \hat{\mathcal{A}}\left[G_{\mathrm{PP}1}(\mathbf{x}_1,\mathbf{x}_2)\ldots G_{\mathrm{PP}N}(\mathbf{x}_{2N-1},\mathbf{x}_{2N})\right]\\ G_{\mathrm{PP}i} &= \psi_i\psi_{\bar{i}} + c_i\psi_{i^*}\psi_{\bar{i}^*}\end{aligned} \quad (21)$$

The significance of this pairing function is that it is capable of describing the static correlations that are most important when chemical bonds are broken. In most uses, the core orbitals are uncorrelated ($c_i = 0$), resulting in the closed-shell generalized valence bond (GVB) wave function of Goddard et al.[140]

The GVB-PP function can be seen as an MCSCF wave function with a particular set of configurations:

$$\Psi_{\mathrm{PP}} = |\Psi_0\rangle + \sum_i c_i|\Psi_{i\bar{i}}^{i^*\bar{i}^*}\rangle + \sum_{i\neq j} c_ic_j|\Psi_{i\bar{i}j\bar{j}}^{i^*\bar{i}^*j^*\bar{j}^*}\rangle + \ldots \quad (22)$$

The relative simplicity of the PP wave function also allows it to be written in the coupled cluster form.[141,142] The coupled cluster approach allows the PP wave function to be determined with relative ease. Presently, there is no method for evaluating the PP wave function apart from its determinant expansion. This expansion includes 2^N determinants, which is substantial, but far less than the factorial number generated in a CASSCF calculation that includes the same set of active orbitals. This limits the use of PP wave functions in QMC to wave functions involving small numbers of active pairs.

3.2. Backflow Transformed Wave Functions

Yet another approach to incorporating correlation effects into an antisymmetric function is to allow the orbitals (or geminals) to depend on the coordinates of the other electrons. This is accomplished by the backflow transformation in which the coordinates of the electrons are modified by a backflow displacement:

$$\Psi_{\mathrm{BF}}(\mathbf{X}) = \Psi_{\mathrm{A}}(\mathbf{X} + \xi) \quad (23)$$

The displacement, ξ, is analogous to the eddies of a classical fluid moving around a large impurity and was first used by Feynman and Cohen to show that the energy of a quantum fluid is minimized by a backflow transformation that conserves the current around the impurity.[143]

The displacement function must be a symmetric function to preserve the overall antisymmetry of Ψ_{A}, but there remains a great deal of flexibility in the form of ξ. For homogeneous systems, it is common for the displacement of electron i to be determined by the sum of pairwise displacements in the directions of the other electrons, j:

$$\xi_i = \sum_j \mathbf{r}_j + \eta(r_{ij})(\mathbf{r}_i - \mathbf{r}_j)$$

where $\eta(r_{ij})$ is a function of interparticle distance. Various forms of $\eta(r_{ij})$, including rational,[144] Gaussian,[124] and polynomial[81] functions, have been suggested. The inhomogeneous backflow function introduced by Lopez-Ríos et al.[81] adds displacements toward nuclei, leading to significantly lower VMC and DMC energies and variances for molecular systems.

3.3. Jastrow Wave Functions

The antisymmetric wave functions in the previous section account for electron correlation indirectly through correlations among the coefficients of the geminal or CI expansions. More compact descriptions of electron correlation are achieved by Jastrow correlation functions that depend explicitly on interparticle distances. The correlation functions, U, can be parametrized in a myriad of ways. U can be partitioned into a hierarchy of terms, $U_1 \ldots U_N$, in which U_N describes correlations among N electrons.

3.3.1. Electron−Nucleus Correlation Functions, U_1. The earliest use of electron−nucleus (e−n) terms in the correlation function were due to Fahy et al.,[145] and a clear discusion of its construction can be found in an earlier review by Foulkes et al.[14]The e−n correlation function does not describe electron correlation per se because it is redundant with the orbital expansion of the antisymmetric function.[145] If the correlation function expansion is truncated at U_1 and the antisymmetric wave function is optimized with respect to all possible variations of the orbitals, then U_1 would be zero everywhere. There remain two strong reasons for including U_1 in the correlation function expansion. First, U_2 depletes more electron density near the nucleus (where the density is high) than in the tail of the wave function (where the density is low). This leads to a net shift of electron density away from the nucleus, which reduces the energetically favorable e−n interactions. The e−n correlation function can be used to readjust the electron density without reoptimizing molecular orbitals.[75,145,146]

Second, the molecular orbitals are typically expanded in Gaussian basis sets that do not satisfy the e−n cusp conditions. The e−n correlation function can satisfy the cusp conditions, but U_1 also influences the electron density in regions beyond the immediate vicinity of the nucleus, so simple methods for determining U_1 solely from the cusp conditions may have a detrimental effect on the overall wave function. Careful optimization of a flexible form of U_1 is required if the e−n cusp is to be satisfied by the one-body correlation function.[128,147]

The basic form of U_1 is a function of the e−n distances, $U_1 = \sum_{i,A} \bar{r}_A(|\mathbf{r}_i - \mathbf{r}_A|)$. An assortment of scaled distance functions, $\bar{r}$, are given in Table 1. The Padé function has a cusp at $r = 0$ that can be adjusted to match the Coulomb cusp conditions by adjusting the a parameter. The Sun form also has a cusp but approaches its asymptotic value far more quickly than the Padé function, which is useful for the linear scaling methods described in section 4. An exponential form proposed by Manten and Luchow is similar to the Sun form but shifted by a constant. By itself, the shift affects only the normalization of the Slater−Jastrow function, but it has other consequences when the function is used to construct more elaborate correlation functions. The polynomial Pade function does not have a cusp, but its value goes to zero at a finite distance.

3.3.2. Two-Electron Correlation Functions, U_2. Two-electron correlations provide the largest contributions to the correlation energy.[151] The simplest e−e correlation functions are spatially homogeneous and depend only on the distances between the electron pairs. However, to satisfy the different cusp conditions for like and unlike spins, the function may have a parametric dependence on spin: $U_2(\mathbf{x}_i,\mathbf{x}_j) = \sum_{i,j} \bar{r}_{\sigma_i\sigma_j}(|\mathbf{r}_i - \mathbf{r}_j|)$. A variety of scaled distance functions are in common use, and several are shown in Table 1. These are the same forms used in the e−n correlation functions, but because the e−e correlation causes electrons to avoid each other while e−n correlation causes electrons to approach nuclei, the multiplicative factors used to scale the interparticle distances will have opposite signs for e−e and e−n correlations.

Inhomogeneous contributions to U_2 can be described by an expansion in powers of the e−e and e−n scaled distance functions.

$$U_2(\mathbf{r}_i,\mathbf{r}_j) = \sum_{mno} \sum_{i<j}^{\text{electrons}} c_{mno}(\bar{r}_{iA}^{\,m}\bar{r}_{jA}^{\,n} + \bar{r}_{iA}^{\,n}\bar{r}_{jA}^{\,m})\bar{r}_{ij}^{\,o} \qquad (24)$$

where we have adopted the shorthand of $\bar{r}_{ij} = \bar{r}(|\mathbf{r}_i - \mathbf{r}_j|)$. This ansatz was first proposed by Boys and Handy (BH),[152] and Schmidt and Moskowitz (SM) later arrived at the same form by considering averaged backflow effects.[153] The SMBH form includes both the e−n function (via the $n = o = 0$ terms) and the homogeneous e−e Jastrow function (via the $m = n = 0$ terms). The remaining e−e−n terms modulate the e−e correlation function according to the e−n distances.

In SM's original work, $\bar{r}$ took the Padé form. Any of the forms in Table 1 are acceptable, but there are qualitative differences between the powers of these functions. If $\bar{r}$ is zero at the origin then $\bar{r}^n$ cannot have a cusp for $n > 1$ and higher powers of $\bar{r}$ can be used to fit longer-range behavior. If $\bar{r}$ is nonzero at the origin, then all powers of $\bar{r}$ can have cusps (if r has a cusp) and higher powers of $\bar{r}$ have decreasing range. Schmidt and Moskowitz used this correlation function to recover ∼75% of the correlation energy for the first row atoms, 25% more than the homogeneous e−e Jastrow.[153]

3.3.3. Filippi−Umrigar Correlation Function. By increasing the number of terms in the BH expansion (SM used physical arguments to select only a subset of the possible terms) and adding terms designed to satisfy the cusp conditions due to the simultaneous approach of two electrons to the nucleus, Filippi and Umrigar obtained between 79% and 94% of the correlation energy for the first-row homonuclear diatomic molecules.[154] The two-electron terms in their correlation function are

Table 1. Scaled Distance Functions, $\bar{r}(r)$; The Coulomb Cusp Condition Is Satisfied by the Parameter Constraints Listed in the Third Column

	$\bar{r}(r)$	cusp
Padé[69]	$(ar)/(1 + br)$	$a = \kappa$
Sun[148]	$-b \exp(-\alpha r)$	$b = \kappa/\alpha$
exponential[149]	$b(1 - \exp(-\alpha r))$	$b = \kappa/\alpha$
polynomial Padé[150]	$[1 - z(r/r_{cut})]/[1 + z(r/r_{cut})]$-$(x) = x^2(6 - 8x + 3x^2)$	n/a

$$U_2 = \frac{b\bar{r}_{ij}}{1 + b'\bar{r}_{ij}} + P(U,S,T) + \bar{F}(U,S,T) + \bar{F}'(U,S,T);$$
$$U = \bar{r}_{ij}; \quad S = \bar{r}_{iA} + \bar{r}_{jA}; \quad T = \bar{r}_{iA} - \bar{r}_{jA} \qquad (25)$$

The function P is a complete fifth-order polynomial of U, S, and T. The terms in the BH expansion are equivalent to those in P, although the polynomial coefficients will differ due to the transformation from $\bar{r}_{iA}$ and $\bar{r}_{jA}$ to S and T. The $\bar{F}$ and $\bar{F}'$ functions are composed of the leading terms in Fock's expansion for the helium atom.

3.3.4. Three-Electron Correlation Functions, U_3. The use of three-electron correlation functions was initially explored by Huang et al.[151] Their study used a complete fifth-order polynomial of the interparticle distances to describe U_3, but the energetic improvements over Filippi and Umrigar's U_2 function were <0.5% for the Li, Be, and Ne atoms studied. The physical interpretation for the limited improvement due to U_3 is that correlations among three or more particles must include at least two particles of the same spin. The antisymmetry of Ψ_A ensures that the wave function approaches zero where two electrons of the same spin meet, so the many-electron density will be very small wherever high-order correlations are most significant. Furthermore, the largest three-body effects are accounted for by products of two-body functions. Most correlation functions are therefore truncated at U_2. Many-body terms such as U_3 are considerably more expensive to compute than U_2 but yield only slight benefits to the accuracy of the calculation, particularly if the results will be refined at the DMC level.

3.3.5. Multi-Jastrow Wave Functions. Although the product form of a SJ wave function has typically been used with a single global Jastrow factor, the benefit of using different Jastrow terms for each molecular orbital of the antisymmetric function was recently demonstrated.[155] The latter approach improves treatment of local electron correlation by facilitating adjustment to the local molecular environment. Also, the nodal structure of the trial wave function can better reflect the parameters of Jastrow functions than the single global Slater−Jastrow wave function. This modification has little effect on the FNDMC eneries for first- and second-row atoms but improves the dissociation energy of HF by 2.4 kcal/mol.

3.4. Trial Wave Function Optimization

Section 2.1 described how the energy of a trial function can be computed by sampling walkers from the electron density, Ψ_T^2, and averaging the local energies of these walkers. The fixed sample optimization method (see, for example, refs 156−158) takes walkers sampled from $\Psi_T^2(\Lambda_0)$, the electron density at the

dx.doi.org/10.1021/cr2001564 |Chem. Rev. 2012, 112, 263–288

initial set of parameter values, to compute the energy (or another optimization criterion) at different values of Λ.

For example, the VMC energy may be rewritten in terms of the fixed sample density by incorporating weights, $w_k = [\Psi^2(\mathbf{X}_k, \Lambda)]/[\Psi^2(\mathbf{X}_k, \Lambda_0)]$ to account for changes of the density due to parameter changes.

$$E(\Lambda) = \frac{\int \Psi_T(\Lambda)\hat{H}\Psi_T(\Lambda)\, d\mathbf{X}}{\int \Psi_T{}^2(\Lambda)\, d\mathbf{X}}$$

$$= \frac{\int \Psi_T{}^2(\Lambda_0)\frac{\Psi_T{}^2(\Lambda)}{\Psi_T{}^2(\Lambda_0)}\frac{\hat{H}\Psi_T(\Lambda)}{\Psi_T(\Lambda)}}{\int \Psi_T{}^2(\Lambda_0)\frac{\Psi_T{}^2(\Lambda)}{\Psi_T{}^2(\Lambda_0)}}$$

$$= \frac{\frac{1}{K}\sum_k w_k(\Lambda)E_{Lk}(\Lambda)}{\frac{1}{K}\sum_k w_k(\Lambda)} \quad (26)$$

Standard multidimensional minimization schemes such as the conjugate gradient method[159] can be then used to minimize $E(\Lambda)$.

Minimization of the Monte Carlo energy estimate minimizes the sum of the exact expectation value and the error due to the finite sample. Although the variational principle provides a lower bound for the energy, there is no lower bound for the error of an energy estimate. Fixed sample energy minimization is therefore notoriously unstable.[75,160] Optimization algorithms based on Newton's, linear, and perturbative methods have been proposed.[75,78,82,161−164]

More suitable optimization functions can be found by using the property that the exact wave function is an eigenfunction of the Hamiltonian. The variance of the local energies of an exact eigenfunction is zero because the local energy is a constant function of $\mathbf{X}$. Accounting for the weights introduced in eq 26, the variance of the local energy as a function of Λ is

$$\sigma^2(\Lambda) = \frac{\sum w_k}{(\sum w_k)^2 - (\sum w_i{}^2)} \sum_k w_k(E_L(X_k, \Lambda) - E(\Lambda))^2 \quad (27)$$

The summands for eq 27 must be positive (or zero) everywhere, so the variance of an approximate wave function is bounded from below by zero, even for a finite sample. The coincidence between the lower bound of the variance and the variance of the exact wave function enables the trial wave function to be optimized by variance minimization. The existence of an absolute lower bound makes variance minimization more robust than energy minimization.[69]

Similar arguments provide grounds for minimizing the absolute deviation of the local energy:[165,166]

$$M(\Lambda) = \frac{1}{K}\sum_k^K w_k(\Lambda)|E_L(X_k, \Lambda) - E(\Lambda)| \quad (28)$$

Like the variance, the mean absolute deviation also has a lower bound of zero, but two arguments suggest that it may be a more effective optimization criterion than the variance. The contribution of each walker to the variance is a quadratic function of the local energy, but its contribution to the absolute deviation has a linear dependence on the local energy. It has been suggested that this difference makes the mean absolute deviation easier to optimize than the variance because the derivative of the absolute value is always ± 1, but the derivative of a quadratic function approaches zero near its minimum. Also, the quadratic contribution of each walker to the variance may allow a few particularly errant walkers to dominate the variance, but the absolute deviation is not as strongly influenced by outlying local energies.

Several authors, including Schmidt and Moskowitz and Greeff and Lester, have explored minimizing the unreweighted variance $\sigma_u{}^2$ of the local energies without accounting for the changes to the density due to changes in Λ.[153,167]

$$\sigma_u{}^2(\Lambda) = \frac{1}{K}\sum_k^K (E_L(X_k) - E(\Lambda))^2 \quad (29)$$

The unreweighted variance does not minimize the variance of $\Psi(\Lambda)$, but it is nevertheless a valid minimization criterion because the variance of the exact wave function will be zero regardless of the distribution of walker coordinates.[168] Renewed interest from Drummond and Needs stems from their observation that the unreweighted variance is sometimes especially easy to minimize.[168] When the only parameters being optimized are linear parameters of the Jastrow function, the unreweighted variance is a quartic polynomial of a single variable. The line-minimization step of conjugate gradient-type algorithms then becomes trivial because the minima of quartic polynomials can be found algebraically.

Snajdr and Rothstein compared a number of properties including average interelectronic distances and multipole moments of wave functions optimized by variance minimization to those optimized by energy minimization.[169] They found that energy-minimized wave functions provided more accurate results for nonenergetic properties. Umrigar and Filippi also found that energy-optimized wave functions have lower energies and higher variances than variance-minimized wave functions.[170] Considering that chemical reactivity is determined by energetic differences and not variance differences, these results suggest that energy minimization should be revisited.

Several new algorithms avoid the pitfalls of fixed sample energy minimization by devising alternative estimates of energy changes due to parameter modifications.[82,170−175] These model energies are constructed from derivatives of the energy of the wave function and do not correspond to the fixed sample energy of eq 26 except when $\Lambda = \Lambda_0$. Unlike the fixed sample energy, the model energies have lower bounds, making them more stable metrics for optimization. This description focuses on the "linear" method of Umrigar et al.,[82] which avoids the computationally demanding step of evaluating second derivatives of the local energy.

The construction of the linear energy model starts from an explicitly normalized expression for the trial wave function.

$$\tilde{\Psi}(\Lambda) = \frac{\Psi(\Lambda)}{\langle\Psi(\Lambda)|\Psi(\Lambda)\rangle^{1/2}} \quad (30)$$

A linearized wave function, $\overline{\psi}(\Lambda)$, is obtained by truncating its Taylor series expansion at first order:

$$\tilde{\Psi}(\Lambda_0 + \Delta) \approx \bar{\Psi}(\Lambda_0 + \Delta)$$

$$= \tilde{\Psi}(\Lambda_0) + \sum_i \frac{\partial\Psi}{\partial\Lambda_i}\Delta_i + \mathcal{O}(\Delta^2) \quad (31)$$

dx.doi.org/10.1021/cr2001564 |Chem. Rev. 2012, 112, 263–288

The initial wave function and its derivatives form a basis set for describing $\overline{\psi}(\Lambda_0 + \Delta)$. When the Hamiltonian and overlap matrices are expanded in this basis, the energy of the linearized wave function becomes

$$\bar{E}(\Delta) = \frac{\langle\bar{\Psi}|\hat{H}|\bar{\Psi}\rangle}{\langle\bar{\Psi}|\bar{\Psi}\rangle} = \frac{\sum_{i,j}\Lambda_i\bar{H}_{ij}\Lambda_j}{\sum_{i,j}\Lambda_i\bar{S}_{ij}\Lambda_j} \quad (32)$$

The minimum of $\bar{E}(\Delta)$ can be found by solving the generalized eigenvalue problem,

$$\sum_j \bar{H}_{ij}\Delta_j = \bar{E}\sum_j S_{ij}\Delta_j \quad (33)$$

which is routinely done using numerical linear algebra software libraries.[176] The solution to eq 33 is then used to update the trial function according to $\Psi(\Lambda) \rightarrow \Psi(\Lambda + \Delta)$.

Eigenvalues of the linearized Hamiltonian also provide estimates of excited-state energies. This property has been used to optimize excited-state wave functions.[177] An state-averaged extension of the linear method optimizes multiple ground- and excited-state wave functions.[178]

3.5. Effective Core Potentials

The purpose of the effective core potential (ECP) approximation is to remove the core electrons from a calculation so that computational effort may be focused on the valence electrons that participate in chemical bonds. Obviously, the ECP must account for changes to the Coulomb potential arising from removal of the core electrons. There must also be a commensurate reduction of nuclear charge. Additional terms are needed to account for the exchange energy and to maintain orthogonality between the valence orbitals and the core orbitals that have been removed. The nonlocality of the latter two terms underlies the unusual form of the ECP:

$$V^{\mathrm{ECP}}(r) = w_{L+1}(r) + \sum_{l=0}^{L}\sum_{m=-l}^{l}|Y_{lm}\rangle(w_{L+1}(r) - w_l(r))\langle Y_{lm}| \quad (34)$$

The value of the ECP depends not only on an electron's coordinates but also on the projection of the wave function for one electron (holding the other electron coordinates constant) onto the spherical harmonics, Y_{lm}. The local term, $w_{L+1}(r)$, depends only on the distance of the electron from the nucleus. The angular potentials w_l are determined so that, beyond some cutoff distance, the "pseudo-orbitals" obtained from an ECP calculation match those of an all-electron calculation but are nodeless and smoothly go to zero within the cutoff radius.[167] The w_l are then fit to a Gaussian expansion[179] so that the potential can be rapidly integrated over Gaussian basis functions.

Some flexibility remains in the selection of terms to be included in this expansion. An assortment of ECPs are possible within this framework because the form of the pseudo-orbital within the cutoff radius is not completely defined. So-called soft ECPs have been designed so that w_l cancels the Coulomb singularity at the nucleus.[180] This is valuable for QMC calculations because their efficiency is sensitive to rapid changes of the potential. Several sets of soft ECPs have been designed specifically for QMC so that Gaussian basis function can be used in QMC calculations without special consideration of the electron−nucleus cusp conditions.[181,182]

Localized ECPs have singularies in the nodal regions of the trial wave function, and the locality approximation is known to lead to numerical instability in DMC calculations. The "T-moves" algorithm provides an alternative to the locality approximation.[183] In this approach, the negative matrix elements of the nonlocal potential are incorporated as an additional displacement step in the random walk, whereas positive matrix elements are simply added to the local potential. T-moves increase the stability of simulations by pushing walkers away from regions where localized ECPs diverge. Also, the T-moves algorithm is variational in the sense that the ground-state energy of the effective Hamiltonian is an upper bound to the exact ground-state energy. More recent work by Casula et al. reduces the time-step error of the original T-moves algorithm and ensures that, for a given time step, the effectiveness of the nonlocal T-moves does not diminish for increasing system size, i.e., it is size-consistent.[184]

There is also lattice-regularized DMC (LRDMC), in which the kinetic term is discretized by a finite difference Laplacian. The regularized Hamiltonian also leads to a variational treatment of nonlocal potentials.[185] The updated version of LRDMC reduced the method's lattice discretization error using an improved effective lattice Hamiltonian.[184] The revised algorithm uses only one lattice size (earlier LRDMC algorithms used two) and has a known leading error term, leading to smoother lattice extrapolation.

4. COMPUTATIONAL CONSIDERATIONS

There is a close connection between advances in ab initio quantum chemistry and the development of computational resources. The tremendous growth of power and availability of high-performance computers has made possible computational studies of increasingly challenging problems. This section provides an overview of QMC scaling properties that are pertinent to parallel computations with any degree of concurrency. Studies of various alternatives to traditional supercomputers and clusters are discussed along with relevant algorithmic improvements and code development efforts.

4.1. Linear Scaling Quantum Monte Carlo

While QMC approaches appeal to quantum chemists primarily for high accuracy, these methods also have computational advantages. The slowest step of a QMC calculation requires $\mathcal{O}(M^3)$ floating point operations (flops) for a molecule of size M, and $\mathcal{O}(M^{1.5})$ steps are needed to achieve a given statistical error. In contrast, the cost of coupled-cluster methods, which are sometimes referred to as the "gold standard" of quantum chemistry, can increase as fast as $\mathcal{O}(M^7)$, which leads to prohibitively expensive calculations for molecules with more than ~12 first-row atoms.[132,186] Because of their reduced scaling and facile adaptation to parallel computers, QMC methods hold special benefits for the evaluation of electronic properties of large molecules. QMC calculations are nevertheless a significant undertaking. The requirement of small statistical errors adds a hefty prefactor to their cost, even for small molecules.

The methods described below reduce these costs so that QMC can be applied to a broader range of molecules. The factors that contribute to the cost of a QMC calculation are discussed. Several of the latter are determined by the statistical nature of the QMC method. The largest of these considerations is the time required to compute the local energy. Linear-scaling computational efforts in energy evaluation can be achieved in recently introduced VMC and FNDMC approaches reformulated in terms of N-particle density matrices.[187]

4.1.1. Scaling Analysis. The vast majority of the computing time consumed in a VMC or DMC calculation is spent evaluating the local energy of the specified trial wave function. The total compute time is roughly the product of T_{Elocal}, the time required for each evaluation of the local energy, and N_{MC}, the number of Monte Carlo points (walkers positions) where the local energy is evaluated. The walkers and the cost of evaluating their local energies are easily distributed among N_{proc} nodes of a parallel computer. There is also a penalty, T_{comm}, incurred for communication between the nodes. The total wall time required to complete a QMC calculation is roughly

$$T_{\mathrm{wall}} = \frac{T_{\mathrm{Elocal}} N_{\mathrm{MC}}}{N_{\mathrm{proc}}} + T_{\mathrm{comm}} \tag{35}$$

The T_{Elocal} and T_{comm} terms can be directly reduced by algorithmic improvements such as those described later in this section. On the other hand, N_{MC} is, to a very large extent, an intrinsic property of the underlying QMC theory. Ceperley[188] has previously analyzed the factors that contribute to N_{MC}. First, the variance of the local energy increases with molecular size, so the number of independent MC points must increase to reduce the error to the same tolerance. Second, the MC points will not be independent from each other until the random walk has taken sufficient steps for the walker positions to decorrelate. Third, the time-step bias of a DMC calculation increases with system size, so a larger number of steps must be taken before the decorrelation time is passed.

Suppose the local energies for a monatomic system have a variance ${\sigma_1}^2$. If the system is enlarged to include M identical, noninteracting atoms, standard error analysis indicates that the variance increases to ${\sigma_M}^2 = M{\sigma_1}^2$. The MC error decreases as $K^{-1/2}$, so if K_1 points are needed to reduce the error bar to an acceptable level for the one-atom system, then $K_M = MK_1$ points are needed to achieve the same error for the M-atom system. For small- and moderate-size molecules, K_M may grow faster than $\mathcal{O}(M)$ because interactions between the atoms cause σ_M to increase.

The number of independent points in the MC average may be less than the total number of points if points sampled by the same walker are serially correlated. A decorrelation time of κ_1 must pass before the local energies of the one-atom system are independent of earlier values. The local energy of the noninteracting M-atom system is just the sum of the local energies of the independent atoms, so that the total energy decorrelates at the same rate as the component energies: $\kappa_M \approx \kappa_1$.

Although the decorrelation time is independent of system size, the degree of serial correlation between steps is determined largely by the time step, τ. DMC calculations require small time steps to maintain reasonable branching factors. Assuming that the local energies are normally distributed with variance of ${\sigma_M}^2$, the average branching factor for the M-atom system is approximately

$$\langle G_{\mathrm{B}} \rangle \approx 1 + \frac{1}{2} M {\sigma_1}^2 {\tau_M}^2 \tag{36}$$

A time step of $\mathcal{O}(M^{-1/2})$ is therefore needed to keep $\langle G_{\mathrm{B}} \rangle$ constant.

The number of independent points required for DMC is found by combining the factors just described.

$$N_{\mathrm{MC}} = K_M * \frac{\kappa_M}{\tau_M} = \mathcal{O}(M) \frac{\mathcal{O}(1)}{\mathcal{O}(M^{-1/2})} = \mathcal{O}(M^{3/2}) \tag{37}$$

Assuming a linear scaling algorithm for the local energy, the compute time for molecular DMC calculations increases at least as fast as $\mathcal{O}(M^{5/2})$. For bulk properties that are reported in energies per atom or per unit cell, the computed energies and errors may both be reduced by $1/M$, so those calculations scale as $\mathcal{O}(M^{3/2})$.

Several measures can be used to reduce the magnitude of N_{MC} (but not its scaling). Trial function optimization decreases N_{MC} in two ways. If the variance of the local energies is reduced then a smaller number of points will be needed to achieve the desired error bar. Reduced variance also permits a larger time step to be used, c.f. eq 36. Effective core potentials decrease the variance of local energies by smoothing the Coulomb potential near the atomic core, thereby reducing N_{MC} via mechanisms similar to those of wave function optimization. Improved random walk algorithms with small time-step errors will also decrease serial correlation.[66,67]

4.1.2. Molecular Orbital Evaluation. The SJ ansatz (see section 3) is the most common type of trial wave function used in QMC. Evaluating the molecular orbitals (MOs) and their derivatives is usually the most time-consuming step in evaluating the local energy for SJ wave functions, requiring up to $\mathcal{O}(N^3)$ flops for an N-electron wave function. An assortment of methods for reducing the cost of MO evaluation to $\mathcal{O}(N)$ have been developed by several groups.[149,189,190]

The Slater matrix for an N-electron determinant will contain N^2 elements consisting of the N occupied orbitals evaluated at each electron's coordinates. If the MOs are expanded using a linear combination of basis functions (i.e., $\phi_i(\mathbf{x}) = \sum_\mu C_{\mu i} \chi_\mu(\mathbf{x})$) and the number of basis functions is $\mathcal{O}(N)$, then $\mathcal{O}(N^3)$ flops are required to evaluate all of the entries in the Slater matrix.

Linear scaling can be achieved when localized MOs (LMOs) are used to create sparsity within the Slater matrix. The density of an LMO is confined to a limited region of space around its centroid, so only a few LMOs need to be evaluated for each electron. The second crux on the way to linear scaling is to accelerate the transformation from basis function to LMOs. Linear scaling QMC methods have been a popular field of research, and several algorithms have been published.

Williamson et al. used maximally localized Wannier functions to express the LMOs[189] that are truncated by setting the value of the orbital to zero outside the sphere containing 99.9% of the orbital density. The transformation from basis functions to MOs is avoided by tabulating the orbitals on a 3-D grid and using a spline procedure for orbital evaluation.

The nonorthogonal LMOs (NOLMOs) of Alfè and Gillan are obtained by dividing the volume of the molecule into a set of overlapping localized regions and maximizing the self-overlap of the orbitals within the localization region.[190] Any part of the orbital outside its localization region is truncated. The transformation step is accelerated by rewriting the LMOs in a basis of "blip" functions. Each blip is nonzero over a small domain so only 64 blips need to be evaluated and transformed.[190]

The first linear scaling QMC method to use Gaussian basis functions was due to Manten and Luchow.[149] They truncated the Boys localized orbitals[191] by neglecting basis functions centered on atoms more than three bond lengths away from the centroid of the LMO. The deletion of basis functions simultaneously reduces both the number of LMOs that must be evaluated and the number of basis functions that must be evaluated and transformed.

The MO evaluation algorithm devised by Aspuru-Guzik et al. truncated the orbital transformation using a numerical cutoff

rather than a spatial one.[192] Their algorithm used a 3-D grid to identify sparsity in the Slater matrix. For each point on the grid, the threshold $C_{\mu i}\chi_\mu(x) > 10^{-12}$ was applied to create a list of relevant coefficients and basis functions. In contrast to the truncation schemes used by other groups, this method neglects the smallest contributions to the MOs instead of the most distant. For large molecules, the grid algorithm is substantially faster than a dense linear transform. However, this grid algorithm performs poorly for small molecules due to irregular memory access patterns.

The NOLMOs used in earlier linear scaling QMC calculations have used finite localization regions to truncate each orbital.[190,193] The "spread" functional used by Liu, Perez-Jorda, and Yang[194] is equivalent to the Boys method for orthogonal orbitals, but in the nonorthogonal case, it minimizes the spatial extent of each orbital rather than maximizing the distance between orbital centers. Liu et al. were able to reduce the spread functional by 83% on average by relaxing the orthogonality constraint, but their minimization algorithm required elaborate procedures to avoid singular transformations.[194]

4.1.3. Correlation Functions. The SMBH function described in section 3.3 is frequently used for its compact and accurate description of inhomogeneous electron correlation.

$$U^{\mathrm{SMBH}} = \sum_A \sum_{mno} \sum_{i<j} c^A_{mno}(\bar{r}_{iA}{}^m \bar{r}_{jA}{}^n + \bar{r}_{iA}{}^n \bar{r}_{jA}{}^m)\bar{r}_{ij}{}^o \qquad (38)$$

Evaluating the SMBH correlation function requires $\mathcal{O}(M^3)$ flops due to the summation over three particles. It can be the rate-limiting step in the evaluation of the local energy even if the BH expansion includes only a modest number of terms.

Manten and Luchow (ML) created a linear scaling algorithm for evaluating the two-body terms in the BH expansion.[149] The short-range scaled distance function used by ML, $\bar{r}^{\mathrm{ML}} = 1 - \exp(-\alpha r_{ij})$, quickly approaches a constant value so that only a linear number of terms in eq 38 need to be evaluated explicitly.

A linear scaling algorithm for evaluation of three-body terms in the BH expansion has been described by Austin et al.[195] Rewriting each term as a trace over a matrix product, $U^A_{mno} = \Sigma_{i\neq j}\bar{r}^m_{Ai}\bar{r}^o_{ij}\bar{r}^n_{jA}$, permitted the use of fast matrix multiplication libraries. Linear scaling was then achieved by taking advantage of the sparsity in the $\bar{r}$ matrices. There is no such sparsity if $\bar{r}^{\mathrm{ML}}$ is used because the asymptotic value of this function is one. To create sparsity, $\bar{r}$ was shifted so that its asymptotic value is zero. The result is identical to the correlation function developed by Sun, Lester, and coworkers (SL),[196] $\bar{r}^{\mathrm{SL}}_{ij} = -\exp(-\alpha r_{ij})$.

4.1.4. Load Balancing. The independent motion of random walkers makes it particularly simple to use parallel computers for QMC calculations. The walker ensembles can be distributed among many processors, and interprocess communication is needed only for occasional averaging. A complication arises in DMC because the branching process can cause unpredictable imbalances in the number of walkers on each processor. This can severely degrade parallel efficiency if processors with fewer walkers must wait for others to complete before continuing past the parallel barrier associated with averaging.

The cost of idle processors increases in significance as petascale computers have tens of thousands of processing cores. To maintain high parallel efficiency, a load-balancing procedure should redistribute walkers after branching. For example, it is possible to send walkers from the processor with the greatest number of walkers to the one with the least until they have the same number of walkers. The process is repeated until all nodes have equal numbers of walkers. This is less than ideal because iterative communication creates multiple communication barriers. The high cost of communication relative to flops magnifies the need for an alternative strategy.

Early versions of the Zori program[197] used a similar approach, but the result of the iterative procedure was computed before any walkers were exchanged; this reduced the amount of communication, but the $\mathcal{O}(N_{\mathrm{proc}}{}^2)$ memory required to store the "transfer matrix" is impractically large when several thousand processors are used. The load-balancing algorithm adopted in more recent versions of the code requires only one global communication step and two $\mathcal{O}(N_{\mathrm{proc}})$ arrays.[198]

5. PARALLELIZATION AND HARDWARE ACCELERATION

Advances in the design of high-performance computing (HPC) systems and the evolution of modern hardware are of immediate relevance, especially in the view of the intrinsic parallelism of QMC. HPC has traditionally been dominated by massively parallel supercomputers connected by custom networks. Clusters of workstations connected by commodity networks also have niches in the HPC community. Hardware accelerators such as graphical processing units (GPUs) and field-programmable gate arrays (FPGAs) are gaining momentum as components of supercomputer and cluster systems.[199−201] Public resource computing has also emerged as an alternative to HPC centers.

The adoption of GPUs in cluster systems has been motivated largely by their high floating-point throughput, high memory bandwidth, and low hardware cost. As supercomputers approach the peta- and exascale, the power demands for running and cooling these systems are driving HPC centers toward GPUs or other hardware architectures that offer more computing and memory resources per watt. The primary impediment to widespread adoption of GPUs for scientific computing is the difficulty of transferring legacy programs to the new architecture. The languages for programming GPUs are often tied to particular hardware platforms, and significant code reorganization and specialized programming models are required to obtain maximum efficiency of the GPU.

Meredith et al. and Anderson et al. have modified versions of their QMC codes to assess the performance of QMC on GPUs.[200,201] GPU hardware accelerated their overall QMC code by a factor of 6; individual kernels achieved speed-ups as large as 30×.[200,201] A study by Weber et al. has also assessed the programming and debugging efforts required to achieve fine-grained parallelism on a variety of GPU-based platforms and languages.[199] The timing data from this QMC application were used to construct a model for predicting the performance of other scientific applications on GPUs. Meredith et al. also compared single-precision GPU results to double-precision CPU results and concluded that the negligibly small differences between the two should not prevent scientifically meaningful results from being obtained from GPU-based QMC codes.[200]

FPGA accelerated systems are being explored as tools for exploiting the polygranular parallelism of the QMC algorithm.[199,202] The most computationally intensive parts of the algorithm are mapped onto reconfigurable FPGA hardware, which allows extensive optimization through pipelining, fine-grained parallelism, and fixed-point arithmetic.[202] The remaining components of the QMC code that are either less demanding or

dx.doi.org/10.1021/cr2001564 |Chem. Rev. 2012, 112, 263–288

offer only coarse-grained parallelism are executed on the CPU. With FPGA hardware acceleration of the wave function and potential energy routines, a 25× speedup was observed relative to a serial reference code.[202] Significant modification of the QMC algorithm was required to obtain accurate results with fixed-point arithmetic; this increases FPGA development costs compared to CPU- and GPU-based systems.

Public resource computing relies on the donation of spare computer time by personal computer owners worldwide. QMC@Home, the first large-scale distributed quantum chemical project, used FNDMC to obtain interaction energies between stacked Watson−Crick DNA base pair complexes (adenine/thymine and cytosine/guanine).[203] By 2008, QMC@Home had access to 15 Tflop/s sustained computing power, rivaling top500 supercomputers of the time for the price of a midsize server. A specially adapted version of the Amolqc[204] software was used for the QMC calculations. Work-scheduling, data-handling, accounting, and community features were provided by Berkeley Open Infrastructure for Network Computing (BOINC) which is based on standard web-server components.[205]

The loosely coupled parallelism of QMC permits efficient use of low cost clusters assembled from a mixed assortment of computing and network hardware. Feldmann et al. used a manager-worker programming model to balance the distribution of walkers among the nodes of a heterogeneous parallel computer.[206] The performance of manager-worker scheme approached the theoretical performance limit of their heterogeneous cluster and performed as well as a conventional algorithm on homogeneous compute systems.

5.1. Advances in Algorithms and Software

Software development is an ongoing process motivated by a wide range of considerations, from improving performance of existing algorithms and implementing new theoretical approaches to exploration of the efficiency of new programming languages.[207] One important factor that is often overlooked by scientific software developers is software accessibility to the general user, so that computations can be set up, executed, and analyzed in a simple and understandable way. Development of friendly graphical user interfaces (GUIs) is becoming an important aspect of the design of production-package scientific software. Introduction of a simple GUI for the Zori QMC software[208] is expected to facilitate a broader use of QMC and provide instructional advantages for students in higher education.[209]

Zori software itself has undergone significant improvements in its latest version.[198] New features of Zori 2.0 include faster wave function evaluation algorithms and robust wave function optimization methods. Optimization procedures were merged into the random walk to streamline the procedure for running VMC calculations. The preparation of Zori input files was simplified by updates to its GUI and user-friendly scripts. Zori 2.0 is an open source program licensed under GPL.

Another QMC software package distributed free of charge is QWalk.[210] QWalk is a state-of-the-art code providing functionality for QMC electronic structure calculations of medium-to-large molecules and solids. The modular form of QWalk encourages and facilitates addition of new features. The current version is highly flexible in the choice of wave function, Hamiltonian, observable, and MC method. QWalk features an efficient parallelization scheme that has been used with up to 10 000 processors.

Even higher concurrencies, up to 100 000 cores, have been achieved with almost perfect parallel efficiency in the CASINO code.[211] With supercomputers achieving petascale performance, such a degree of parallelism opens new venues for QMC applications and is perceived as critical for addressing problems that cannot be tackled by other ab initio methods due to conceptual or technical limitations. CHAMP[212] and QMCPACK[213] are among other QMC software packages that are available for use by communities at large.

The efficiency of various stages of QMC algorithms is constantly being improved. For example, a strategy for the generation of the ensemble of random walkers has been designed[214] that shortens the equilibration phase of QMC simulations and reduces the total run time. Improved algorithms for updating trial wave functions[215,216] provide speed and storage savings that facilitate the treatment of large systems with multideterminant wave functions. Alternative sampling strategies that lead to better statistical and computational properties of VMC calculations have been proposed.[217] An increase of computational power facilitates QMC computations of such large scales that the supply of psueudo-random numbers may be exhausted during production-quality runs. Stochastic simulations of such intensity raise the bar for the quality of (pseudo)-random number generators (RNGs). The performance of several RNGs in VMC and DMC calculations was evaluated[218] to ascertain numerical reliability of the results.

6. APPLICATIONS

This section summarizes the range of computations that have been performed using QMC. Considering availability of earlier reviews,[7,13,15] we focus on the work done in the past five years. The key aspects of the computational methodologies used in these studies are presented together with their main findings.

The traditional strength of QMC methods in determining accurate absolute energies is reflected by the number of studies dedicated to atomic, molecular, and reaction energetics, including ionization potentials, electron affinities, and inter- and intramolecular binding energies. Recent progress with the RQMC and AFQMC methods has contributed to more active pursuit of properties that do not commute with the Hamiltonian. Recent advances in QMC methodologies facilitate studies that have targeted selected molecular properties in addition to energies, including electron densities, equilibrium geometries, and transition moments.

6.1. Ground-State Systems

Ground-state QMC calculations are the most abundant. Preparation of trial wave functions of excited states in VMC faces the same difficulties as standard orbital-based methods. In DMC, there are no bounds for excited states analogous to the variational principle for the ground state. No tiling theorem exists in FNDMC treatment of excited states. The availability of accurate experimental data and, especially in the case of small systems, computational results from alternative ab initio approaches makes atoms and molecules in their ground states ideal targets for testing and benchmarking QMC techniques. The aspects of QMC currently being tested vary—from the application of different types of basis sets to new importance sampling strategies.[219]

The main challenge for improving the accuracy of FNDMC calculations is to improve the quality of the nodes of trial wave functions. This objective motivates investigations of novel optimization methods[220,221] and tests of more flexible trial wave functions. Considerable effort has therefore been expended in the pursuit of understanding the fundamental structure of nodal

surfaces.[84,86,89,222,223] For example, Bressanini and Morosi examined the algebraic structure of RHF, UHF, and GVB wave functions for the ground state of the N atom and showed that the nodes of any one of these wave functions could be reproduced by either of the other two forms.[73] Although this result seems to indicate that variational optimization of a given trial function form might not minimize the DMC energy for that form, studies that have reoptimized the parameters of multideterminant wave functions in the presence of a Jastrow factor have observed consistent decreases in the DMC energy for larger active spaces.[75,76]

Computational efficiency has also stimulated modifications to tailor ECPs and their corresponding basis sets for QMC (see section 3.5). Relativistic ECPs and relativistic approximations within QMC are critically important to understanding the chemistry of transition metals and heavy elements.[224]

As noted in section 2.1, DMC samples a mixed distribution, which introduces a bias for calculations of properties that do not commute with the Hamiltonian. This issue has been addressed in studies of expectation values of multipole moments,[63,225] differential operators,[226,227] relativistic corrections,[228] and Born−Oppenheimer forces on nuclei.[229] Methods for sampling the "pure" density must overcome the increased variance and higher computational demands associated with computing the weighting factors that correct for the mixed distribution. Vrbik has proposed a scheme for computing derivatives of the DMC energy from the mixed density by analyzing the serial correlation of walker weights.[230] In addition, a new sampling method based on the Hellmann−Feynman theorem has been developed to sample a large class of operators diagonal in real space, including densities and interaction energies, exactly within FNDMC.[231]

Estimators of operators other than the Hamiltonian suffer from substantial fluctuations, and the zero-variance principle does not hold. Variance can be reduced by construction of new estimators that decrease fluctuations without biasing the resulting estimate.[232,233] The calculation of forces is particularly sensitive to the magnitude of the variance because estimators are related to derivatives of the total energy. Various aspects of force calculations have been investigated, including their sensitivity to whether the trial function satisfies the electron−nucleus cusp condition,[234] the effect of Pulay's correction in calculations based on the Hellmann−Feynman theorem,[235] and the applicability of adjoint algorithmic differentiation.[236] A stochastic line-minimization algorithm relying on Bayesian inference was devised to find precise structural minima.[237] A series of papers by Badinski and co-workers have made significant andvances toward evalulating the Pulay terms in the expressions for the forces for systems with nonlocal pseudopotentials in DMC,[238−241] including accurate estimates for "nodal terms"[240] and force estimates that use zero-variance properties to improve statistical efficiency.[238]

Mixed estimators are avoided in the RQMC approach discussed in section 2.5. Recent developments have increased the efficiency of RQMC for large systems.[114] An assessment of electron distributions in atoms and molecules showed that "no-compromise" RQMC achieved the highest accuracy among a variety of QMC methods.[242] The AFQMC method has demonstrated excellent performance in the traditionally challenging description of stretched bonds and a related issue of spin-contamination.[243]

6.1.1. Atoms. Ground-state energies of positive and negative ions of elements from Li to Ar have been characterized using all-electron nonrelativistic FNDMC to address challenges of adequate and consistent treatment of correlation effects in systems with varying charges and numbers of electrons. A comparison of computed ionization potentials and electron affinities with experimental values validated the computed results.[244]

All-electron VMC and DMC calculations of the ground-state energies of first-row atoms enabled assessment of trial wave functions of four types: single-determinant SJ, multideterminant SJ, single-determinant SJ with backflow transformations, and multideterminant SJ with backflow transformations. The DMC method with backflow-transformed multideterminant SJ trial wave functions recovered 99% or more of the correlation energy for Li, Be, B, C, N, and Ne, 97% for O, and 98% for F.[245]

All-electron and pseudopotential VMC and DMC calculations of the ground-state energies of Ne and Ne^+ were used to gauge the effect of trial wave function quality.[246] The SJ wave functions with HF orbitals, optimized orbitals, and orbitals transformed to include backflow correlations were used. The HF orbitals give nearly optimal single-determinant nodal surfaces for the ground states of Ne and Ne^+. Backflow-transformed wave functions yielded the most accurate results for both VMC and DMC, although the computational cost per move in VMC and DMC increased by a factor of between 4 and 7. In comparison to backflow transformation, orbital optimization slightly improved VMC energies but had very little effect on the DMC results for this system. All QMC calculations, irrespective of the form of the trial wave function, the type of the QMC method, the use of all-electron basis sets, or pseudopotentials, led to excellent agreement with the experiment for the Ne IP. Even in the worst case of VMC nonrelativistic pseudopotential calculations, the error was only 0.60(3)% of the IP value.[246]

All-electron ground-state energy calculations of 3d transition-metal atoms were carried out to obtain accurate correlation energies. This work relied on the FN approximation to domain Green's function Monte Carlo (FN GFMC).[247] Application of QMC to such systems is traditionally challenging due to large fluctuations induced by core electrons and complicated atomic shell structure leading to inhomogeneous charge distributions.

Relativistic ECPs provide a comparatively easy way to include a simplified accounting for some relativistic effects in QMC calculations. If relativistic effects are very large, then relativistic ECPs are inadequate.[248] In ref 249, relativistic contributions to the total energies of Cu and Cu^+ were evaluated as differences between Dirac−Fock and Hartree−Fock energies. Electron correlation effects were obtained using nonrelativistic DMC calculations.

Theoretical consistency requires a simultaneous treatment of the relativistic and correlation effects.[250] This can be achieved if relativistic local energies are used in the QMC simulations. A new all-electron relativistic VMC approach was proposed to address this problem.[251] The relativistic local energy was derived from the zeroth-order relativistic approximation (ZORA) Hamiltonian. The IPs of the first-row atoms were computed to demonstrate that along with relativistic effects the method recovers electron correlations at the same level as nonrelativistic QMC. An electron−nucleus cusp correction scheme for ZORA-QMC was proposed[252] to extend the nonrelativistic correction scheme.[253] The new scheme replaces the MOs of the SJ wave function with an exponential-type correction function and improves the stability of computations with both STOs and GTOs.

6.1.2. Molecules. Harkless and Irikura used VMC and DMC to address the challenges of computing an accurate dissociation energy for Be_2. Their approach used a CASSCF trial function to

account for the near-degeneracies among the 2s and 2p states of Be.[254] A variety of active spaces and strategies for truncating the CAS expansion were explored to assess the sensitivity of FNDMC to perturbations of the trial wave function. The best agreement between FNDMC and experiment was obtained when the active space included the valence electrons and the orbitals with the closest energies. Larger active spaces resulted in significantly larger dissociation energies that were attributed to inadequate optimization of trial wave functions with large numbers of determinants.

The performance of VMC and FNDMC in the prediction of ground-state energies and derived properties, such as dissociation energies and ionization potentials, of a range of small molecules (Li_2, Be_2, H_2O, NH_3, CH_4, and H_2CO) has been benchmarked. The focus of the study[255] was the effect of STOs and of the size of Jastrow correlation function in the Boys−Handy form. With the single-reference trial wave functions without reoptimization of orbital parameters, fixed-node energies were found to lie within 95% of the estimated exact values and to within 1% of reported values. It was shown that systematic inclusion of two- and three-body terms in the Jastrow factor is also important for QMC calculations of molecular systems.

A phaseless AFQMC study of bond stretching in the BH and N_2 molecules and an H_{50} chain has been reported. A trial wave function based on UHF orbitals was sufficient to produce potential curves in agreement with experimental, CCSD(T), and DMRG data. At large separations the AFQMC approach led to more uniform behavior and higher accuracy than CCSD(T) except at a few stretched configurations. Problematic cases were completely resolved with MCSCF trial wave functions.[256]

The extended linear optimization method has enabled robust simultaneous optimization of large numbers of linear and nonlinear parameters of the trial wave function.[221] Using this method, Toulouse and Umrigar optimized the basis function exponents, orbital coefficients, CAS coefficients, and Jastrow parameters for the ground state of C_2. The C_2 FNDMC potential energy curve was size-consistent with a spin-restricted single-determinant SJ trial wave function, but the spin symmetry of the system was broken at the dissociation limit. However, the correct spin symmetry and size consistency were preserved in both VMC and FNDMC calculations with CAS-SJ trial functions.

To resolve a recent controversy over the stability of an elusive covalently bound O_4 species, a FNDMC study was performed.[257] A single HF determinant was insufficient to obtain accurate nodes and led to considerable errors in both the heat of formation and the dissociation barrier height compared to the best available reference data. The problem was resolved with a CASSCF trial wave function truncated according to size of CI coefficients. The values obtained for the heat of formation agreed with existing ab initio benchmarks, supported the reliability of this type of trial function, and provided confidence in the calculated barrier values. The DMC findings indicate that a chemically bound O_4 species should be detectable experimentally.[257]

Performance of single-reference versus multireference wave functions and canonical orbitals versus natural orbitals from CI with single and double excitations were compared in a VMC/FNDMC study of bond dissociation energies for symmetric and asymmetric arrangements of S_4.[258] For single-reference trial functions, orbital choice had a noticeable effect on the absolute and relative energies, particularly for DMC. Proper description of the dissociation required a multireference wave function. The choice of orbitals was less significant for multireference wave functions.

The energetics of the isomerization reaction of bicyclobutadiene were obtained at the FNDMC level of theory. This reaction involves a biradical species that typically poses a significant challenge to most ab initio approaches.[259] Static and dynamic correlation contribute differently to the product and reactant molecules, so the multireference trial wave function must include a carefully selected set of CSFs for a balanced description of electron correlation in both systems. As few as three CSFs were sufficient for adequate error cancellation in this system. Overall, FNDMC findings were in closer agreement with experiment than CCSD(T) results.

An accurate OH bond dissociation energy in phenol was established from DMC calculations using single-determinant SJ trial wave functions. The findings were 87.0 ± 0.3 kcal/mol (HF orbitals) and 87.5 ± 0.3 kcal/mol (Kohn−Sham orbitals). The experimental values range from 86 to 90 kcal/mol, and orbital-based theories predicted energies range from 86 to 91 kcal/mol.[260]

FNDMC and DFT were used to predict the growth mechanism for a molecular line of styrene on a hydrogenated silicon surface.[261] The two approaches agreed that an intra-dimer-row growth model was preferred over an inter-dimer-row model. The predicted adsorption/reaction energies and barrier heights, however, differed considerably. The study showed that, for surface reactions, DFT predictions should be interpreted with caution and that FNDMC provides a viable alternative for large systems.

The adiabatic positron affinities of HCN and LiH were recently obtained from FNDMC calculations.[262] The study relied on a product form of the trial wave function with multicomponent electron-positron determinant and a Jastrow factor including two- and three-body terms. The electron−positron and positron−nucleus cusp conditions were imposed with a Jastrow factor. Electron MOs were modified to satisfy the electron−nucleus cusp condition. Agreement between the DMC result for LiH and existing benchmark data supported the credibility and adequacy of the chosen theoretical framework for small positronic molecules. The DMC result predicted positron binding to HCN to be 20× stronger than that from HF theory, indicating that correlation effects are important to the description of weakly bound positronic molecular compounds.

The FNDMC method with new scalar-relativistic soft-core Hartree−Fock ECPs was used to obtain potential curves around the equilibrium geometries of selected dimers and diatomic hydrides, namely, As_2, Br_2, Sb_2, I_2, and XH (X = Ga, Br, In, I, and At), to determine the equilibrium bond lengths and vibrational frequencies using polynomial fits. These results were consistent with those of CCSD(T) and supported the use of a new family of scalar-relativistic ECPs constructed by Burkatzki, Filippi, and Dolg (BFD) to obtain an accurate account of relativistic effects.[248]

A family of small vanadium oxide molecules was characterized with respect to their ionization and atomization energies and oxygen abstraction.[263] The FNDMC results obtained with soft ECPs and Gaussian basis functions were not significantly different from all-electron FNDMC calculations with cusp-corrected bases. The study showed that, for transition-metal systems, more accurate results are obtained with trial wave functions from generalized-gradient approximation (GGA) rather than hybrid density functionals. In the cases where experimental data are available, the accuracy of FNDMC results was comparable to CCSD(T) predictions.

A family of porphyrin complexes with several transition metals was investigated using FNDMC. All-electron basis sets with both

large-core and small-core ECPs were employed.[264] Stable DMC runs were obtained only with nondivergent large-core Trail-Needs ECPs.[265] The results showed a pronounced dependence of metal-porphyrin binding energies on the metal atom basis set. Significant (~0.8 eV) variation between DMC, hybrid DFT, and HF values was reported.[264]

The efficiency, precision, and accuracy of all-electron VMC and FNDMC calculations were tested in a study of 55 molecules from the G2 set[266] using Slater-type basis sets to construct HF and DFT determinants for trial wave functions. Electron−nucleus cusp conditions were enforced. The performance gain of STO over GTO was estimated to be 45%. On average, 95% of the correlation energy was recovered in DMC calculations. Atomization energies were reproduced with a mean average deviation of 3.2 kcal/mol from the experimental values.

6.1.3. Weakly Bound Systems. The availability of "exact" FMC results for the He_2 potential energy curve[267] makes this an ideal system for studying the influence of trial functions on FNDMC calculations for weakly bound systems. The FNDMC method has been found to yield a highly accurate energy of He_2 and the dipole/induced-dipole interaction energy for He−LiH.[268] A later investigation of the potential curve of helium dimer demonstrated that VMC with a SJ trial wave function is unable to account for correlation effects responsible for van der Waals (vdW) bonding.[269] The FNDMC treatment, on the other hand, yielded results in close agreement with existing theoretical values even though the trial wave function was less accurate than that used in an earlier VMC calculation.[268] Further improvement in the binding energy of this system was achieved with RQMC computations using a single-determinant SJ trial wave function optimized by a stochastic reconfiguration method.[270]

Despite being the simplest molecular assembly pertinent to aqueous solvation effects, the water dimer already poses significant computational challenges. The equilibrium dissociation energy of water dimer has been computed using all-electron FNDMC.[271] The trial wave functions in the SJ form used a single Slater determinant from either HF or hybrid DFT calculations with atomic natural orbital (ANO) basis sets. The molecular orbitals were modified to satisfy the electron−nucleus cusp condition. The results of these FNDMC calculations matched existing experimental data and results of coupled cluster calculations within the FNDMC statistical error (0.18 kcal/mol). No significant sensitivity of the equilibrium dissociation energy to the type of the trial wave function was observed. An extension of this study addressed the effect of ECPs and backflow corrections.[272] The effect of the locality approximation and the "T-moves" algorithm in the ECP treatment were also examined. The time step errors of the T-moves algorithm are larger than those from the locality approximation. The errors cancel, however, when energy differences are taken, such as for the dissociation energy.

A systematic investigation of binding between two benzene rings in face-to-face and parallel displaced geometries has been reported.[273] A QMC framework was devised that facilitates reliable description of interactions driven by vdW forces. The LRDMC approach was used with a highly correlated Jastrow-AGP (JAGP) trial wave function. A strategy for overcoming the lack of size consistency of JAGP ansatz was proposed. The trial wave function was optimized using the stochastic reconfiguration technique. Agreement between the experimental and computational results illustrated QMC's ability to accurately describe weak intermolecular attractions.

A detailed study of molecular hydrogen adsorption on benzene[274] compared JAGP (VMC and LRDMC) and SJ single-determinant product form (FNDMC) wave functions. The QMC methods achieved agreement within 0.2 mhartree among each other and agreed with earlier CCSD(T) and MP2 results. The LRDMC approach was also used to perform bonding analysis by comparing charge densities of the molecular complex and the noninteracting molecules. The change of electron density near the equilibrium distance showed the formation of static dipoles, indicating that the binding mechanism is not based solely on vdW forces.

Potential energy curves for a water−benzene complex were obtained using a variety of the most popular computational methods.[275] Agreement between DMC and CCSD(T) curves was reported. Differences on the order of 20−30 meV were attributed to fixed-node error.

The performance of DFT in the description of weak interactions was evaluated by comparison to FNDMC and RQMC results for complexes of various molecules and benzene.[276] The DFT electron densities were found to be in good agreement with those from accurate RQMC results. The approximate description of exchange effects in DFT was demonstrated to have a significant impact on binding energies. Strategies for improvement upon existing shortcomings of exchange-correlation approximations were discussed. QMC computations of exact behavior of electron densities in realistic environments were suggested as a viable metric for guiding such improvements.

A comparative study of the quality of FNDMC and standard-, hybrid-, and meta-GGA functionals description of a nanoscale MgH_2 cluster[277] showed mixed performance of DFT across cluster sizes. In general, the results strongly suggested that it is critically important to benchmark DFT with highly accurate and reliable methods when nanoscale metal hydride structures are treated.

QMC calculations were performed to obtain an accurate treatment of electron correlation in the binding of NO_2 to carbon nanotubes (CNTs) and to resolve discrepancies between MP2 and DFT results.[278] Findings from VMC and FNDMC with single-determinant and multideterminant trial wave functions of SJ form showed weak binding of two adsorbate molecules, suggesting that charge transfer is not involved in the binding of these systems. These results imply an alternative explanation of the experimentally observed conductivity changes in CNT-based molecular sensors.

An FNDMC study with a single-determinant SJ wave function utilizing Trail-Needs ECPs addressed the issue of relative stability of two polymorphs of a *para*-diiodobenzene molecular crystal. The DMC results improve upon inconclusive and inconsistent results from DFT and predict higher stability of the α-phase relative to the β-phase at zero temperature. The study emphasizes the importance of an accurate treatment of noncovalent interactions by accurate accounting of electron correlation.[279]

DMC calculations for 1-D and 2-D homogeneous electron gases (HEGs) were used to obtain accurate binding energies for pairs of thick parallel metal wires.[280] The DMC results showed significant quantitative differences from random-phase approximation (RPA) calculations and completely disagreed with the standard pairwise vdW model. The data obtained can serve as benchmarks in future theoretical studies and in parametrization of model interactions.

Insights into the nature of binding between graphite layers were gained from VMC and LRDMC and a single-determinant Slater−Jastrow trial wave function.[281] For the first time, the

binding energy and long-range behavior of the total energy were characterized. The computed "cleavage energy" required to separate graphene layers agreed with the latest experimental data within 6 meV/atom. A power law for variation of the interaction energy with interlayer separation was derived that is close to one found for two semiconducting planes.

Periodic longitudinal chains of hydrogen molecules served as a generic model of a periodic system in FNDMC calculations of linear and nonlinear susceptibilities.[282] The importance of such calculations for systems where DFT traditionally fails was emphasized. The feasibility of accurate DMC calculations was demonstrated, and excellent agreement with the most accurate ab initio results was found.

FNDMC and complete basis set MP2 results served as reference data in an examination of the ability of exchange correlation density functionals to describe hydrogen bonds and van der Waals interations in water hexamers.[283] Four low-energy isomers of the water clusters were studied. The DMC and MP2 calculations predicted the same energy ordering for the isomers and agreed on the dissociation energy differences (excluding zero-point corrections) within 4 meV/H_2O. The total (nonstatistical) error in the DMC calculations due to the FNA and pseudopotential localization approximation were estimated to be ~10 meV/H_2O. None of the exchange correlation functionals predicted the correct energy ordering or the correct minimum energy isomer.

The experimental crystal structure of the nitrate−triazine−triazine complex has an unusual asymmetrical geometry in which the π-stacked triazine rings are staggered and not perfectly faced and the nitrate ion is off-center and tilted with respect to the nearest triazine ring.[284] The interactions that lead to these structural features were explored with dispersion-corrected density functional theory (DCDFT) and FNDMC calculations.[285] Binding between this complex was attributed not only to the anion−π and $\pi-\pi$ interactions but also to a cooperative anion−$\pi-\pi$ effect. DCDFT routinely identified qualitatively similar minimum energy geometrie, but consistently overestimated binding energies relative to MP2 and DMC. This study included a constrained optimization of a chloride−triazine complex at the DMC level using correlated sampling; the equilibrium chloride−centroid distance was indistinguishable from the distance predicted by MP2.

6.1.4. Solvent Effects: QMC/MD and Embedding Methods. The treatment of large systems can be tremendously simplified if they can be represented as composed of fragments whose reliable description requires different levels of accuracy. A broad range of embedding techniques facilitate very accurate but more computationally demanding treatment of a chemically relevant fragment while the remaining fragments are treated at a less expensive lower level.

Hydration of selected atomic ions was studied by means of VMC simulations to test a new theoretical model for polarization effects within a continuum model in the framework of nonlinear response theory.[286] The computed free energies of polarization were in good agreement with estimates derived from experiment. A particular case of spherical solutes was considered with strategies outlined for generalization to nonspherical solutes. The dielectric continuum model was later extended to nonspherical solvents by Amovilli et al.,[287] and the new method was validated by comparison to HF and DFT continuum solvent models for a collection of small molecules and anions.[287]

A mean field embedding scheme for QMC was proposed by Flad et al.[288] Orbital localization is used to separate a QMC active region from the rest of the system. The two regions were coupled by introducing nonlocal effective potentials into the Hamiltonian.

The first implementation of a QMC/MD approach was reported by Grossman and Mitas.[289] Nuclear trajectories were generated in DFT/MD simulations, and accurate DMC energies were obtained for regularly sampled nuclear configurations. It was found that only three DMC steps were necessary to update the walker positions for each step along the nuclear paths. As a result, the QMC component of the simulation increased the overall computer time only by a factor of 2. Despite large variance in the QMC energies at each step, very small error bars for thermodynamic properties were achieved by averaging over the entire run. The study reported the value of the heat of water evaporation to be 9.1(4) kcal/mol, in excellent agreement with the experimentally measured value of 9.9 kcal/mol. (The DFT estimate is ~30% too low.)

To facilitate application of QMC approaches to the description of chemical reactions in the condensed phase, an explicit solvent model was developed for QMC in the framework of a hybrid approach combining quantum mechanics and molecular mechanics (QM/MM).[290] The solute and the most relevant solvent molecules are treated at VMC or FNDMC level, and a force-field is used for the remaining solvent molecules. Coupling between the QMC and MM regions was achieved via a standard coupling Hamiltonian, modified to avoid collapse of walkers on nuclei of the MM part. The resulting QMC/MM approach with TIP3P model of water was tested in calculations of water−dimer binding energies in different configurations along with some selected water-solvated complexes. Introduction of QMC for the QM part was shown to yield significant improvement in accuracy and to produce results in excellent accord with other ab initio approaches. It is anticipated that QMC/MM hybrids will facilitate large-scale QMC/MD simulations.

Implementation of QMC with fragment molecular orbitals (FMOs) facilitates an equally accurate but less demanding treatment of large systems.[291] The efficiency and accuracy of the VMC-FMO method was demonstrated in a study of the total energy of a glycine trimer.

Very recently, Attaccalite and Sorella[292] carried out QMC/MD calculations with QMC forces for liquid hydrogen and evaluated its properties under various thermodynamic conditions. Molecular dynamics methods compatible with VMC and PIMC have also been introduced.[293]

6.1.5. Properties Other Than the Energy. Transition-metal chemistry is abundant and computationally challenging. A FNQMC study of oxides of the five first transition-metal atoms (Sc, Ti, V, Cr, and Mn) aimed to characterize their binding energies, equilibrium geometries, and dipole moments. FNDMC with single-determinant trial wave functions provided remarkably accurate results, which were on average 50% better than available meta-GGA and CCSD(T) results. The same conclusion applies to interatomic distances, which were obtained by means of Bayesian fitting. More challenging calculations of the dipole moment were performed using RQMC. The results reinforce the view that trial wave functions with accurate nodes are needed to achieve agreement with experimental data.[150]

Some of the difficulty of eliminating trial function bias from DMC calculations of expectation values of nondifferential operators that do not commute with the Hamiltonian can be overcome with RQMC (see section 2). RQMC was used to study a variety of ground-state properties of a water molecule, such as dipole moment, components of the quadrupole moment tensor, and

diamagnetic shielding.[294] SCF guiding functions of varying quality were benchmarked to gain insights on how the accuracy of the expectation values was affected by nodes. The advantages of the head−tail adjusted RQMC algorithm were demonstrated.

The influence of electron correlation on the expectation values of the electron density, the intracule density, the extracule density, their respective Laplacians, and the two forms of kinetic energy density was revealed in a VMC study of hydrogen molecule.[295] VMC calculations with explicitly correlated wave functions were performed for three values of the interatomic separation and clearly confirmed the traditional description of this system as a combination of covalent and ionic structures. Substantial differences between the properties studied and the HF calculations were found.

New local estimators for assigning electron and spin densities to nuclei were tested in VMC simulations of several first-row atoms and selected heavy elements (Ar and K).[296] The problem of evaluating properties with infinitely local estimators and unbounded variances was addressed by introducing appropriate sampling strategies. Improved computational efficiency was achieved with respect to alternative computational schemes.

Efficient QMC estimators for extracule and intracule densities were derived.[297] The bond-length dependence of electron correlation effects along the dissociation curve of hydrogen molecule was studied with their help. Anisotropic correlation effects were demonstrated to accompany the localized increase of the correlation energy at stretched geometries. A small long-range part of the Coulomb hole was found at the equilibrium bond length.

An investigation of long-range asymptotic behavior of the electron density of nonrelativistic two-electron He-like ions combined DFT and numerical DMC simulations. This approach made possible considerable analytic progress in the description of the problem.[298]

The origin of the collapse of the 3.3 μm CH stretching band in the unidentified infrared (UIR) bands of polyaromatic hydrocarbons upon ionization was investigated in a comparative study relying on MRCISD and FNDMC formalisms.[299] Electric dipole moments of the neutral CH fragment in the ground electronic state and its cation in the ground and first electronic excited state were calculated to assess the scaling of IR intensities. DMC calculations were carried out with a full-valence CAS wave function, expanded in STOs, and multiplied by two- and three-body Jastrow factors. In QMC, the dipole moment is more sensitive to imperfections of trial wave function than total energies. A new hybrid estimate for the dipole moment was proposed that combines DMC and VMC estimates and has a more favorable sytematic bias that is linear in the fixed-node error but quadratic in the error in the wave function. Results of MRCISD and FNDMC were in agreement with each other and led to an interpretative model for predicting the strength of the respective band of neutral or ionized PAHs.

6.2. Excited-State Properties

QMC calculations of excited states that are the lowest of a given symmetry are straightforward. It is more challenging to obtain excited states of the same symmetry as a lower state. No theorem exists that insures that such a calculation evolves to the appropriate state. An early calculation of the $(E^1S_g^+)$ state of H_2 using a MCSCF trial function was the first example of FNDMC to successfully address this problem.[300] Challenging calculations of excited states for small hydrocarbon systems have been carried out by Schautz and Filippi.[301,302] These systems present particularly difficult computational challenges due to the fact that they exhibit a number of near-degenerate excited states and require precise treatment of electron correlation. Careful optimization of the variational trial functions for ground and excited states enabled the authors to identify the correct excitations within the given symmetry types and to compute accurate energy differences.

An approach to field-free calculations of polarizabilities of excited states has been proposed by Li et al.[303] The VMC method was used to optimize trial wave functions of the three lowest singlet and triplet states of S, P, and D symmetry of helium atom.[304] The electric dipole oscillator strengths for all possible 1S-1P, 1P-1D, 3S-3P, and 3P-3D transitions were calculated with these explicitly correlated wave functions. The next most important operator, the electric quadrupole, was calculated to enable computation of oscillator strengths for all possible 1S-1D, 1P-1P, 1D-1D, 3S-3D, 3P-3P, and 3D-3D transitions of the helium atom.[305] A favorable relationship between the quality of the results and the compactness of the trial wave function was demonstrated. It was noticed that reduction of fluctuations of the local multipole operators around the origin is necessary for accurate oscillator strength calculations.

A large set of electronic states of scandium dimer was characterized using a variety of ab initio methods to establish its ground state.[306] FNDMC calculations used a product form of the trial wave function with a UHF determinant, relativistic ECPs, and associated basis sets. States of the same spatial symmetry but different multiplicity were treated at the DMC level. In contrast to the general assumption of a quintet ground state, DMC and CASPT2 predicted a triplet state to be the most stable.

The low-lying electronic excited states of dinitrogen (N_2) were characterized by QMC computations of their respective vertical excitation energies.[307] Various strategies for generating trial wave functions were compared. Optimization of the independent-particle part of the trial wave functions was avoided in the interest of simplicity and robustness. On the basis of comparison to available experimental data, the least favorable performance was given by VMC calculations with single-determinant and multideterminant CISD trial wave functions. The best performance was demonstrated in the case of VMC and DMC calculations with CASSCF trial wave functions.

As an alternative to the FNDMC approach, excited states can be efficiently treated by AFQMC.[308] Potential energy curves of the ground state and two low-lying singlet excited states of C_2 were computed. Accurate results were obtained with truncated CASSCF trial wave functions without further optimization. Small basis set AFQMC calculations agreed with full CI calculations; large basis set calculations matched experimental values of spectroscopic constants.

The ground state of methylene and its three lowest adiabatic excited states were studied.[309] Jastrow−Slater multideterminant trial wave functions for VMC and FNDMC computations were generated from increasing CASSCF expansions. Simultaneous optimization of Jastrow, CSF, and orbital parameters essentially eliminated dependence of the DMC excitation energies on active space size. Lower excited states were accurately characterized even with the smallest CAS, which suggested that static correlation effects have the most important effects on the nodes.

In a systematic investigation of photoisomerization of model retinal chromophores,[310] QMC was used to facilitate a balanced description of static and dynamic correlation effects and test generally accepted results of CASSCF calculations. The study featured VMC and FNDMC vertical excitations energies of several chromophores and geometry optimization of the ground and excited states of the

dx.doi.org/10.1021/cr2001564 |Chem. Rev. 2012, 112, 263–288

model systems at the VMC level. It was noted that accurate VMC gradients required optimization of all wave function parameters in an energy-minimization scheme. The results obtained suggest the need to reinvestigate the photoisomerization mechanism of the retinal chromophore in the gas phase and protein environments using methods more reliable and accurate than CASSCF.

The singlet vertical transition of acrolein, involving an oxygen lone pair and antibonding p-orbital of CO fragment, provided insight into the contribution of various factors to the fixed-node error.[311] Minimal and extended CASSCF expansions were used to construct trial functions. Orbital optimization was performed in state-specific CASSCF calculations and compared to a common set of optimized orbitals from state-averaged CASSCF. Three basis sets of increasing size were employed. Extensive benchmarking involved all possible combinations of the aforementioned parameters. A very simple strategy that relied on a basis set ab initio wave function and no QMC optimization of orbital parameters was sufficient to obtain very accurate energies of electronic transitions in CO.

Vertical excitation energies of neutral and anionic forms of the green fluorescent protein (GFP) chromophore were computed with TD-DFT, EOM-CC, CASPT2, and FNDMC.[178] For the anionic species, the CASPT2 and DMC calculations converged quickly with the size of the CAS expansion, and all computational methods agreed within 0.12 eV. Agreement among the theoretical methods and a Kamlet−Taft fit to solution-phase absorption data raised concerns about the accuracy of gas-phase photodestruction spectroscopy for these systems. The neutral molecule required significantly large CAS expansions for the CASPT2 calculations to converge and the discrepancy among the methods is larger, ∼0.5 eV.

Dubecký et al. computed the S_0-S_1 vertical excitation energies of the cis and trans isomers of azobenzene using FNDMC.[312] The trial wave function was obtained from a CASSCF calculation with a (14,12) active space, truncating the configuation expansion to include a vastly recuced number of determinants, and reoptimizing the truncated CAS wave function in the presence of a Jastrow factor. This more compact wave function allowed the experimental results to be reproduced with chemical accuracy. A novel metric of nodal differences between wave functions was also developed and used to show that the truncated CAS wave functions provide better initial guesses for VMC optimization than DFT.

Send et al. used FNDMC, CASPT2, third-order coupled cluster linear response theory (exCC3), and TDDFT to generate a set of benchmark values for the lowest vertical excitation energies of a series of cyanine dyes.[313] For all methods, the excitation energy decreased smoothly as the dye molecules increased in size. Except for the smallest cyanine, DMC excitation energies were largest among ab initio values, followed by exCC3 and CASPT2. The maximum difference between CASPT2 and DMC excitation energies was 0.34 eV. TDDFT with the B2PYLP function gave remarkable agreement with DMC. The significant discrepancy between the theoretical and experimental excitation energies was attributed to nonvertical transitions.

6.3. General Theory

The electron localization function (ELF) is a popular and powerful tool for analyzing electronic densities in terms of bonding elements. The electron pair localization function (EPLF) is a counterpart of ELF suitable for analyzing QMC ensembles.[314] EPLF is a simple and practical tool that can be used with QMC to identify regions that maximize the probability of finding electron pairs.[315] Such regions bear close resemblance to ELF domains or domains of orbital localization.

An ELF-QMC study investigated the potential of several molecules as amination agents. Equilibrated FNDMC ensembles were analyzed in terms of several modified EPLF functions. The modifications were intended to enhance the ability to discern nitrogen lone pairs and estimate their volumes. It was proposed that integrals of EPLFs can be used to distinguish between nucleophilic and electrophilic systems.[316]

The influence of correlation on the interpretation and origin of Hund's multiplicity rule was investigated in a systematic QMC study of various atoms.[317,318] From FNDMC results, it was concluded that the stability of the highest spin-multiplicity originated from enhancement of the electron−nucleus attraction energy.

QMC simulations have also helped to reveal connections between fluctuations of charge in atomic domains and bond orders.[319] Mueller et al.'s approach used Baders's analysis of HF densities to identify atomic domains and then used DMC to ascertain bond orders. Comparison of DMC and HF bond orders facilitated quantification of correlation effects. Significant reduction of bond orders of Lewis covalent bonds upon incorporation of electron correlation was reported, along with enhancement of bond orders between nonbonded atoms.

The exchange-correlation energy density of a series of small molecules was evaluated in a study that combined a coupling-constant integration procedure and VMC.[320] Comparison of "exact" QMC results with LDA predictions revealed that the spatial variation of errors in LDA XC energy essentially followed the sign and shape of the Laplacian of electron density. This finding led to the conclusion that improved models for XC functional should incorporate the Laplacian of the electron density.

A combined study of kinetic and potential contributions to the correlation energy of H_2 was performed using VMC and DMC.[321] The spatial changes discerned in the electron density distribution were demonstrated to agree with the correlation virial theorem and the electrostatic theorem. The study emphasized the role of the correlational virial theorem as the most important guiding principle in the investigation of electron correlation effects in molecules and solids.

The VMC capability to inexpensively evaluate complicated integrals was recently used in a study of the performance of the Boys−Handy transcorrelated (TC) equation for Jastrow factors.[322] Test calculations demonstrated that the TC approach is a viable alternative to F12 methods.

7. CONCLUSION

In this review, we presented an overview of QMC methods for the electronic structure of atoms, molecules, and molecular assemblies. The coverage included basic theoretical aspects, considerations of computational efficiency, and QMC's practical applicability to a wide range of chemical problems. The latter include ground- and excited-state properties. The fixed-node QMC (FNDMC) was discussed and emphasized owing to the exceptional accuracy, reliability, and robustness of the method. Until recently, applications of QMC method were limited to small systems of light atoms. Recent developments and results clearly indicate the feasibility of the QMC computations for large systems that are beyond the reach of other ab initio methods.

Recent progress in algorithms, the growth of computational power and the inherent parallelism of QMC are pivotal to overcoming limitations imposed by the statistical nature of QMC calculations. Even large systems in challenging chemical contexts can be

simulated with chemical accuracy. Methodological advances have eased the application of QMC in its different forms to electronic properties besides the energy. The ability of QMC to evaluate quantum operators for wave functions that cannot be integrated analytically remains a major strength of the approach. This capability has facilitated significant contributions of the QMC method to fundamental understanding of the electronic wave function and its properties. The rigorous theoretical underpinning for QMC translates into reliable results that may serve as reference data for calibrating other methods.

8. OUTLOOK

The following considerations are pertinent to the future of QMC methods. The fermion sign problem has yet to be resolved. The fixed-node approximation to DMC recovers from 90% to 95% of the correlation energy and therefore captures enough many-body effects to predict cohesive energies, barrier heights, optical gaps, and similar quantities within a few percent of experiments. The missing correlation is nevertheless crucial for subtle effects such as magnetic phenomena, differences between near-degenerate states, and macroscopic quantum phenomena such as superconductivity.

Another issue is the development of methods suitable for efficient application to very large systems. The challenge here is to construct more efficient and accurate representations the many-body wave function. Advances in this area will also stimulate progress in QMC-based dynamical methods. QMC approaches that treat nuclear and electronic degrees on the same footing remain an open area of research. A separate aspect of future QMC progress is the availability of user-friendly software packages that provide all the necessary capabilities, from generation of trial wave functions to statistical analysis and visualization of the results.

AUTHOR INFORMATION

Corresponding Author

*E-mail: walester@lbl.gov. Phone: (510) 643-9590. Fax: (510) 642-1088.

Present Addresses

[§]National Energy Rearch Scientific Computing, Lawrence Berkeley National Laboratory

BIOGRAPHIES

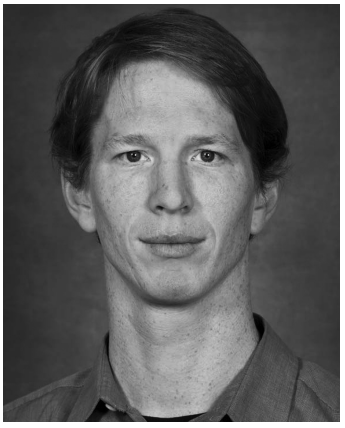

Brian Austin received his B.A. degree from Reed College and his Ph.D. in Chemistry from The University of California at Berkeley. His graduate research included algorithmic improvments for quantum Monte Carlo. He is currently a postdoctoral fellow at the National Energy Research Scientific Computing Center. His research focuses on the development of parallel algorithms and numerical optimization.

Dr. Dmitry Yu. Zubarev received his Ph.D. degree from Utah State University in 2008. His thesis focused on theoretical photoelectron spectroscopy of gas-phase molecular clusters and development of a generalized model of chemical bonding in these systems, under the supervision of Professor Alex Boldyrev. Currently Dr. Zubarev is working as a postdoctoral associate with Professor William A. Lester at the University of California, Berkeley. His main area of research is application of quantum Monte Carlo to simulation of photoelectron spectra and x-ray absorption spectra of molecules and molecular assemblies, such as solute−solvent complexes.

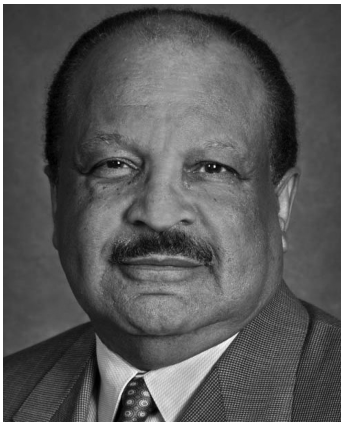

William A. Lester, Jr., was born in Chicago, Illinois, in 1937 and earned degrees in Chemistry from the University of Chicago in 1958 and 1959. In 1964 he was awarded the Ph.D. in Chemistry from The Catholic University of America with research in the area of theoretical chemistry carried out at the National Bureau of Standards under the direction of Dr. Morris Krauss. He subsequently joined the group of Professor Richard B. Bernstein at the Theoretical Chemistry Institute and the Department of Chemistry, University of Wisconsin, Madison, with concurrent service as Assistant Director of the Institute and Lecturer in the Department of Chemistry. In 1968 he joined the IBM Research Laboratory in San Jose, California, followed in 1978 by selection as Director, U.S. National Resource for Computation in Chemistry, and concurrently Associate Director,

Lawrence Berkeley National Laboratory. In 1981, he was appointed Professor of Chemistry, University of California, Berkeley. In 2010, he was appointed Professor of the Graduate School at Berkeley. His research interests were earlier on collision dynamics and, more recently, on the electronic structure of molecular systems with emphasis in the latter on the quantum Monte Carlo method.

ACKNOWLEDGMENT

B.M.A. was supported by the Petascale Initiative in Computational Science at the National Energy Research Scientific Computing Center, which is supported by the Office of Science of the U.S. Department of Energy under contract number DE-AC02-05CH11231. D.Yu.Z. was supported by the National Science Foundation under grant NSF CHE-0809969. W.A.L. was supported by the Director, Office of Energy Research, Office of Basic Energy Sciences, Chemical Sciences, Geosciences and Biosciences Division of the U.S. Department of Energy, under contract number DE-AC03-76F00098.

REFERENCES

(1) Hammond, B. L.; Lester, W. A., Jr.; Reynolds, P. J. *Monte Carlo Methods in Ab Initio Quantum Chemistry: Quantum Monte Carlo for Molecules*; World Scientific: Hackensack, NJ, 1994.
(2) Metropolis, N.; Ulam, S. J. *Am. Stat.* **1949**, *44*, 335.
(3) Kalos, M. H. *Phys. Rev.* **1962**, *128*, 1791.
(4) Anderson, J. B. *J. Chem. Phys.* **1975**, *63*, 1499.
(5) Schmidt, K. E. *Conference on Models and Methods in Few Body Physics*, 1986
(6) Lester, W. A., Jr.; Hammond, B. L. *Annu. Rev. Phys. Chem.* **1990**, *41*, 283.
(7) Aspuru-Guzik, A.; Kollias, A. C.; Salomon-Ferrer, R.; Lester, W. A., Jr. In *Handbook of Theoretical and Computational Nanotechnology*; Rieth, M., Schommers, W., Eds.; American Scientific Publishers: Valencia, CA, 2005.
(8) Ceperley, D. M.; Mitas, L. In *New Methods in Computational Quantum Mechanics*; Prigogine, I., Rice, S. A., Eds.; John Wiley and Sons: New York,1996.
(9) Acioli, P. H. *J. Mol. Struct.* **1997**, *394*, 75.
(10) Bressanini, D.; Reynolds, P. J. In *Monte Carlo Methods in Chemical Physics*; Ferguson, D. M., Siepmann, J. I., Truhlar, D. G., Eds.; Wiley: New York, 1998; p 247.
(11) Mitas, L. In *Quantum Monte Carlo Methods in Physics and Chemistry*; Nightingale, M. P., Umrigar, C. J., Eds.; Klewer Academic Publishers: 1998.
(12) Anderson, J. B. In *Reviews in Computational Chemistry*; Lipkowitz, K. B., Boyd, D. B., Eds.; John Wiley and Sons: New York, 1999; Vol. 13, p 133.
(13) Luchow, A.; Anderson, J. B. *Annu. Rev. Phys. Chem.* **2000**, *51*, 501.
(14) Foulkes, W. M. C.; Mitas, L.; Needs, R. J.; Rajagopal, G. *Rev. Mod. Phys.* **2001**, *73*, 33.
(15) Aspuru-Guzik, A.; Lester, W. A., Jr. In *Computational Chemistry*; Le Bris, C., Ed.; Elsevier: Amsterdam, The Netherlands, 2003; p 485.
(16) Towler, M. D. *Phys. Status Solidi B* **2006**, *243*, 2573.
(17) Koonin, S. E.; Meredith, D. C. *Computational Physics, FORTRAN version*; Addison Wesley: Boston, MA, 1995.
(18) Gould, H.; Tobochnik, J. *An Introduction to Computer Simulation Methods*; Addison Wesley: Boston, MA, 1996.
(19) Thijssen, J. M. *Computational Physics*; Cambridge University Press: Cambridge, U.K., 1999.
(20) Ceperley, D. M. *Rev. Mod. Phys.* **1995**, *67*, 279.
(21) Sarsa, A.; Schmidt, K. E.; Magro, W. R. *J. Chem. Phys.* **2000**, *113*, 1366.
(22) Benoit, D. M.; Clary, D. C. *J. Chem. Phys.* **2000**, *113*, 5193.
(23) Kwon, Y.; Huang, P.; Patel, M. V.; Blume, D.; Whaley, K. B. *J. Chem. Phys.* **2000**, *113*, 6469.
(24) Clary, D. C. J. *Chem. Phys.* **2001**, *114*, 9725.
(25) Viel, A.; Whaley, K. B. *J. Chem. Phys.* **2001**, *115*, 10186.
(26) Viel, A.; Coutinho-Neto, M. D.; Manthe, U. *J. Chem. Phys.* **2007**, *126*, 024308.
(27) Li, Z.; Wang, L.; Ran, H.; Xie, D.; Blinov, N.; Roy, P. N.; Guo, H. *J. Chem. Phys.* **2008**, *128*, 224513.
(28) Hinkle, C. E.; McCoy, A. B. *J. Phys. Chem. A* **2008**, *112*, 2058.
(29) Beslic, I.; Markic, L. V.; Boronat, J. *J. Chem. Phys.* **2008**, *128*, 064302.
(30) Silva, G. M. E.; Gargano, R.; da Silva, W. B.; Roncaratti, L. F.; Acioli, P. H. *Int. J. Quantum Chem.* **2008**, *108*, 2318.
(31) Li, H.; Blinov, N.; Roy, P.-N.; Le Roy, R. J. *J. Chem. Phys.* **2009**, *130*, 144305.
(32) Coccia, E.; Bodo, E.; Gianturco, F. A. *J. Chem. Phys.* **2009**, *130*, 094906.
(33) Petit, A. S.; McCoy, A. B. *J. Phys. Chem. A* **2009**, *113*, 12706.
(34) Hinkle, C. E.; McCoy, A. B. *J. Phys. Chem. Lett.* **2010**, *1*, 562.
(35) Ceperley, D. M.; Alder, B. J. *Phys. Rev. Lett.* **1980**, *45*, 566.
(36) Alet, F.; Capponi, S.; Laflorencie, N.; Mambrini, M. *Phys. Rev. Lett.* **2007**, *99*, 117204.
(37) Maezono, R.; Ma, A.; Towler, M. D.; Needs, R. J. *Phys. Rev. Lett.* **2007**, *98*, 025701.
(38) Kolorenc, J.; Mitas, L. *Phys. Rev. Lett.* **2008**, *101*, 185502.
(39) Casula, M.; Ceperley, D. M.; Mueller, E. J. *Phys. Rev. A* **2008**, *78*, 033607.
(40) Nie, F.-M.; Demeshko, S.; Fuchs, S.; Dechert, S.; Pruschke, T.; Meyer, F. *Dalton Trans.* **2008**, 3971.
(41) Clark, B. K.; Ceperley, D. A. *Comput. Phys. Commun.* **2008**, *179*, 82.
(42) Shorikov, A. O.; Korotin, M. A.; Streltsov, S. V.; Skornyakov, S. L.; Korotin, D. M.; Anisimov, V. I. *J. Exp. Theor. Phys.* **2009**, *108*, 121.
(43) Binnie, S. J.; Sola, E.; Alfe, D.; Gillan, M. J. *Mol. Simul.* **2009**, *35*, 609.
(44) Sola, E.; Alfe, D. *Phys. Rev. Lett.* **2009**, *103*, 078501.
(45) Esler, K. P.; Cohen, R. E.; Militzer, B.; Kim, J.; Needs, R. J.; Towler, M. D. *Phys. Rev. Lett.* **2010**, *104*, 185702.
(46) Gandolfi, S.; Pederiva, F.; Fantoni, S.; Schmidt, K. E. *Phys. Rev. Lett.* **2007**, *98*, 102503.
(47) Wiringa, R. B.; Pieper, S. C.; Carlson, J.; Pandharipande, V. R. *Phys. Rev. C* **2000**, *62*, 014001.
(48) Varga, K.; Pieper, S. C.; Suzuki, Y.; Wiringa, R. B. *Phys. Rev. C* **2002**, *66*, 034611.
(49) Bauer, W. *J. SIAM* **1958**, *6*, 438.
(50) Hammersley, J. M.; Handscomb, D. C. *Monte Carlo Methods (Methuen's Monographs on Applied Probability & Statistics)*; Methuen: 1965.
(51) Halton, J. H. *SIAM Review* **1970**, *12*, 1.
(52) Wood, W. W.; Erpenbeck, J. J. *Annu. Rev. Phys. Chem.* **1976**, *27*, 319.
(53) McDowell, K. *Int. J. Quantum Chem.* **1981**, *Suppl. 15*, 177.
(54) Kalos, M. H.; Whitlock, P. A. *Monte Carlo methods. Vol. 1: Basics*; Wiley-Interscience: New York, 1986.
(55) Sobol, I. M. *A Primer for the Monte Carlo Method*; CRC Press: 1994.
(56) Fishman, G. *Monte Carlo*; Springer: New York, 2003.
(57) Manno, I. *Introduction to the Monte Carlo Method*; Akademiai Kiado: Budapest, Hungary, 1999.
(58) Doucet, A., de Freitas, N., Gordon, N., Smith, A., Eds. *Sequential Monte Carlo Methods in Practice*; Springer-Verlag: New York, 2001.
(59) Liu, J. S. *Monte Carlo Strategies in Scientific Computing*; Springer-Verlag: New York, 2001.
(60) Metropolis, N.; Rosenbluth, A. W.; Rosenbluth, M. N.; Teller, A. H.; Teller, E. *J. Chem. Phys.* **1953**, *21*, 1087.
(61) Assaraf, R.; Caffarel, M. *Phys. Rev. Lett.* **1999**, *83*, 4682.
(62) Ceperley, D. M.; Bernu, B. *J. Chem. Phys.* **1988**, *89*, 6316.

(63) Barnett, R. N.; Reynolds, P. J.; Lester, W., Jr. *J. Comput. Phys.* **1991**, *96*, 258.
(64) Einstein, A. *The collected papers of Albert Einstein*; Princeton University Press: Princeton, N.J., 1987.
(65) Assaraf, R.; Caffarel, M.; Khelif, A. *Phys. Rev. E* **2000**, *61*, 4566.
(66) Umrigar, C. J.; Nightingale, M. P.; Runge, K. J. *J. Chem. Phys.* **1993**, *99*, 2865.
(67) DePasquale, M. F.; Rothstein, S. M.; Vrbik, J. *J. Chem. Phys.* **1988**, *89*, 3629.
(68) Ceperley, D. M. In *Recent Progress in Many-Body Theories*; Zabolitzky, J. G., de Llano, M., Fortes, M., Clark, J. W., Eds.; Springer: Berlin, 1981.
(69) Umrigar, C. J.; Wilson, K. G.; Wilkins, J. W. *Phys. Rev. Lett.* **1988**, *60*, 1719.
(70) Curtiss, L. A.; Jones, C.; Trucks, G. W.; Raghavachari, K.; Pople, J. A. *J. Chem. Phys.* **1990**, *93*, 2537.
(71) Grossman, J. C. *J. Chem. Phys.* **2002**, *117*, 1434.
(72) Flad, H. J.; Caffaral, M.; Savin, A. In *Recent Advances in Quantum Monte Carlo Methods*; Lester, W. A., Jr., Ed.; World Scientific: Singapore, 1997; p 73.
(73) Bressanini, D.; Morosi, G. *J. Chem. Phys.* **2008**, *129*, 054103.
(74) Bressanini, D.; Morosi, G.; Tarasco, S. *J. Chem. Phys.* **2005**, *123*, 204109.
(75) Toulouse, J.; Umrigar, C. J. *J. Chem. Phys.* **2007**, *126*, 084102.
(76) Toulouse, J.; Umrigar, C. J. *J. Chem. Phys.* **2008**, *128*, 174101.
(77) Ortiz, J. V.; Weiner, B.; Ohrn, Y. *Int. J. Quantum Chem.* **1981**, 113.
(78) Casula, M.; Sorella, S. *J. Chem. Phys.* **2003**, *119*, 6500.
(79) Domin, D.; Braida, B.; Lester, W. A., Jr. *J. Phys. Chem. A* **2008**, *112*, 8964.
(80) Bajdich, M.; Mitas, L.; Drobný, G.; Wagner, L. K.; Schmidt, K. E. *Phys. Rev. Lett.* **2006**, *96*, 130201.
(81) Lopez-Ríos, P.; Ma, A.; Drummond, N. D.; Towler, M. D.; Needs, R. *J. Phys. Rev. E* **2006**, *74*, 066701.
(82) Umrigar, C. J.; Toulouse, J.; Filippi, C.; Sorella, S.; Hennig, R. G. *Phys. Rev. Lett.* **2007**, *98*, 110201.
(83) Reynolds, P. J.; Dupuis, M.; Lester, W. A., Jr. *J. Chem. Phys.* **1985**, *82*, 1983.
(84) Ceperley, D. M. *J. Stat. Phys.* **1991**, *63*, 1237.
(85) Glauser, W. A.; Brown, W. R.; Lester, W. A., Jr.; Bressanini, D.; Hammond, B. L.; Koszykowski, M. L. *J. Chem. Phys.* **1992**, *97*, 9200.
(86) Bressanini, D.; Reynolds, P. J. *Phys. Rev. Lett.* **2005**, *95*, 110201.
(87) Cances, E.; Jourdain, B.; Lelievre, T. *Math. Models Methods Appl.* **2006**, *16*, 1403.
(88) Ceperley, D. M.; Alder, B. J. *J. Chem. Phys.* **1984**, *81*, 5833.
(89) Bianchi, R.; Bressanini, D.; Cremaschi, P.; Morosi, G. *Comput. Phys. Commun.* **1993**, *74*, 153.
(90) Bianchi, R.; Bressanini, D.; Cremaschi, P.; Morosi, G. *Chem. Phys. Lett.* **1991**, *184*, 343.
(91) Bianchi, R.; Bressanini, D.; Chremaschi, P.; Morosi, G. *J. Chem. Phys.* **1993**, *98*, 7204.
(92) Ceperley, D. M.; Kalos, M. H. In *Monte Carlo methods in statistical physics*; Binder, K., Ed.; Springer-Verlag: Berlin, 1979.
(93) Kalos, M. H.; Pederiva, F. In *Quantum Monte Carlo Methods in Physics and Chemistry*; Nightingale, M. P., Umrigar, C. J., Eds.; Springer: New York, 1999.
(94) Arnow, D. M.; Kalos, M. H.; Lee, M. A.; Schmidt, K. E. **1982**, *77*, 5562.
(95) Anderson, J. B.; Traynor, C. A.; Boghosian, B. M. *J. Chem. Phys.* **1991**, *95*, 7418.
(96) Zhang, S.; Kalos, M. H. *Phys. Rev. Lett.* **1991**, *67*, 3074.
(97) Kalos, M. H.; Pederiva, F. *Phys. Rev. Lett.* **2000**, *85*, 3547.
(98) Anderson, J. B. *J. Chem. Phys.* **1992**, *96*, 3702.
(99) Diedrich, D. L.; Anderson, J. B. *Science* **1992**, *258*, 786.
(100) Bajdich, M.; Tiago, M. L.; Hood, R. Q.; Kent, P. R. C.; Reboredo, F. A. *Phys. Rev. Lett.* **2010**, *104*, 193001.
(101) Reboredo, F. A.; Hood, R. Q.; Kent, P. R. C. *Phys. Rev. B* **2009**, *79*, 195117.
(102) Reboredo, F. A. *Phys. Rev. B* **2009**, *80*, 125110.
(103) Baer, R.; Head-Gordon, M.; Neuhauser, D. *J. Chem. Phys.* **1998**, *109*, 6219.
(104) Baer, R. *Chem. Phys. Lett.* **2000**, *324*, 101.
(105) Zhang, S. W.; Krakauer, H. *Phys. Rev. Lett.* **2003**, *90*, 136401.
(106) Zhang, S.; Krakauer, H. *Phys. Rev. Lett.* **2003**, *90*, 136401.
(107) Al-Saidi, W. A.; Zhang, S.; Krakauer, H. *J. Chem. Phys.* **2006**, *124*, 224101.
(108) Al-Saidi, W. A.; Krakauer, H.; Zhang, S. *J. Chem. Phys.* **2007**, *126*, 194105.
(109) Al-Saidi, W. A.; Krakauer, H.; Zhang, S. *J. Chem. Phys.* **2006**, *125*, 154110.
(110) Liu, K. S.; Kalos, M. H.; Chester, G. V. *Phys. Rev. A* **1974**, *10*, 303.
(111) Reynolds, P. J.; Barnett, R. N.; Hammond, B. L.; Grimes, R. M.; Lester, W. A., Jr. *Int. J. Quantum Chem.* **1986**, *29*, 589.
(112) Caffarel, M.; Claverie, P. *J. Chem. Phys.* **1988**, *88*, 1088.
(113) Baroni, S.; Moroni, S. *Phys. Rev. Lett.* **1999**, *82*, 4745.
(114) Yuen, W. K.; Farrar, T. J.; Rothstein, S. M. *J. Phys. A* **2007**, *40*, F639.
(115) Yuen, W. K.; Oblinsky, D. G.; Giacometti, R. D.; Rothstein, S. M. *Int. J. Quantum Chem.* **2009**, *109*, 3229.
(116) Booth, G. H.; Alavi, A. *J. Chem. Phys.* **2010**, *132*, 174104.
(117) Cleland, D.; Booth, G. H.; Alavi, A. *J. Chem. Phys.* **2010**, *132*, 041103.
(118) Booth, G. H.; Thom, A. J. W.; Alavi, A. *J. Chem. Phys.* **2009**, *131*, 054106.
(119) Christov, I. P. *Opt. Exp.* **2006**, *14*, 6906.
(120) Christov, I. P. *J. Chem. Phys.* **2007**, *127*, 134110.
(121) Christov, I. P. *J. Chem. Phys.* **2008**, *129*, 214107.
(122) Christov, I. P. *J. Chem. Phys.* **2008**, *128*, 244106.
(123) Christov, I. P. *J. Phys. Chem. A* **2009**, *113*, 6016.
(124) Holzmann, M.; Ceperley, D. M.; Pierleoni, C.; Esler, K. *Phys. Rev. E* **2003**, *68*, 046707.
(125) Andrews, S. B.; Burton, N. A.; Hillier, I. H.; Holender, J. M.; Gillan, M. *J. Chem. Phys. Lett.* **1996**, *261*, 521.
(126) Slater, J. C. *Phys. Rev.* **1930**, *36*, 57.
(127) Davidson, E. R.; Feller, D. *Chem. Rev.* **1986**, *86*, 681.
(128) Ma, A.; Towler, M. D.; Drummond, N. D.; Needs, R. J. *J. Chem. Phys.* **2005**, *122*, 224322.
(129) Petruzielo, F. R.; Toulouse, J.; Umrigar, C. J. *J. Chem. Phys.* **2010**, *132*, 094109.
(130) Junquera, J.; Paz, O.; Sánchez-Portal, D.; Artacho, E. *Phys. Rev. B* **2001**, *64*, 235111.
(131) Harrison, R. J.; Fann, G. I.; Yanai, T.; Gan, Z.; Beylkin, G. *J. Chem. Phys.* **2004**, *121*, 11587.
(132) Head-Gordon, M. *J. Phys. Chem.* **1996**, *100*, 13213.
(133) Helgaker, T.; Jorgensen, P.; Olsen, J. *Molecular Electronic-Structure Theory*; Wiley: New York, 2000.
(134) Szabo, A.; Ostlund, N. S. *Modern Quantum Chemistry*; Courier Dover Publications: 1996.
(135) Bartlett, R. *Annu. Rev. Phys. Chem.* **1981**, *32*, 359.
(136) Shaik, S. S.; Hiberty, P. C. *A Chemist's Guide to Valence Bond Theory*; Wiley: New York, 2007.
(137) Klein, D. J., Trinajstic, N., Eds. *Valence Bond Theory and Chemical Structure*; Elsevier: 1990.
(138) Cooper, D. L. *Valence bond theory*; Elsevier: 2002.
(139) Bouchaud, J. P.; Georges, A.; L'huillier, C. *J. Phys. (Paris)* **1988**, *49*, 553.
(140) Goddard, W. A., III; Dunning, T. H., Jr.; Hunt, W. J.; Hay, P. J. *Acc. Chem. Res.* **1973**, *6*, 368.
(141) Cullen, J. *Chem. Phys.* **1996**, *202*, 217.
(142) Voorhis, T. V.; Head-Gordon, M. *J. Chem. Phys.* **2001**, *115*, 7814.
(143) Feynman, R. P.; Cohen, M. *Phys. Rev.* **1956**, *102*, 1189.
(144) Kwon, Y.; Ceperley, D. M.; Martin, R. M. *Phys. Rev. B* **1993**, *48*, 12037.
(145) Fahy, S.; Wang, X.; Louie, S. *Phys. Rev. Lett.* **1988**, *61*, 1631.
(146) Umezawa, N.; Tsuneyuki, S. *J. Chem. Phys.* **2004**, *121*, 7070.

(147) Drummond, N. D.; Towler, M. D.; Needs, R. J. *Phys. Rev. B* **2004**, *70*, 235119.
(148) Huang, S. Y.; Sun, Z. W.; Lester, W. A., Jr. *J. Chem. Phys.* **1990**, *92*, 597.
(149) Manten, S.; Luchow, A. *J. Chem. Phys.* **2003**, *119*, 1307.
(150) Wagner, L. K.; Mitas, L. *J. Chem. Phys.* **2007**, *126*, 034105.
(151) Huang, C. J.; Umrigar, C. J.; Nightingale, M. P. *J. Chem. Phys.* **1997**, *107*, 3007.
(152) Boys, S. F.; Handy, N. C. *Proc. R. Soc. London, Ser. A* **1969**, *310*, 43.
(153) Schmidt, K. E.; Moskowitz, J. W. *J. Chem. Phys.* **1990**, *93*, 4172.
(154) Filippi, C.; Umrigar, C. J. *J. Chem. Phys.* **1996**, *105*, 213.
(155) Bouabca, T.; Braida, B.; Caffarel, M. *J. Chem. Phys.* **2010**, *133*, 044111.
(156) Z.W., S.; Huang, S.; Barnett, R.; Lester, W., Jr. *J. Chem. Phys.* **1990**, *93*, 3326.
(157) Bressanini, D.; Morosi, G.; Mella, M. *J. Chem. Phys.* **2002**, *116*, 5345.
(158) Bressanini, D.; Reynolds, P. J. *Advances in Chemical Physics*; John Wiley & Sons, Inc.: New York, 2007; p 37.
(159) Press, W. H.; Teukolsky, S. A.; Vetterling, W. T.; Flannery, B. P. *Numerical Recipes in C*; Cambridge University Press: Cambridge, U.K., 1992.
(160) Nightingale, M. P.; Melik-Alaverdian, V. *Phys. Rev. Lett.* **2001**, *87*, 043401.
(161) Lin, X.; Zhang, H.; Rappe, A. *J. Chem. Phys.* **2000**, *112*, 2650.
(162) Casula, M.; Attaccalite, C.; Sorella, S. *J. Chem. Phys.* **2004**, *121*, 7110.
(163) Sorella, S. *Phys. Rev. B* **2001**, *64*, 024512.
(164) Luo, H.; Hackbusch, W.; Flad, H.-J. *J. Chem. Phys.* **2009**, *131*, 104106.
(165) Aspuru-Guzik, A. Solving Schrodinger's Equation Using Random Walks, Ph.D. thesis, U. C. Berkeley, Berkeley, CA, 2004.
(166) Bressanini, D.; Morosi, G.; Mella, M. *J. Chem. Phys.* **2002**, *116*, 5345.
(167) Greeff, C. W.; Lester, W. A., Jr. *J. Chem. Phys.* **1998**, *109*, 1607.
(168) Drummond, N. D.; Needs, R. *J. Phys. Rev. B* **2005**, *72*.
(169) Snajdr, M.; Rothstein, S. M. *J. Chem. Phys.* **2000**, *112*, 4935.
(170) Umrigar, C. J.; Filippi, C. *Phys. Rev. Lett.* **2005**, *94*, 150201.
(171) Filippi, C.; Fahy, S. *J. Chem. Phys.* **2000**, *112*, 3523.
(172) Schautz, F.; Fahy, S. *J. Chem. Phys.* **2002**, *116*, 3533.
(173) Prendergast, D.; Bevan, D.; Fahy, S. *Phys. Rev. B* **2002**, *66*, 155104.
(174) Sorella, S. *Phys. Rev. B* **2005**, *71*, 241103.
(175) Scemama, A.; Filippi, C. *Phys. Rev. B* **2006**, *73*, 241101.
(176) Angerson, E.; Bai, Z.; Dongarra, J.; Greenbaum, A.; Mckenney, A.; Du Croz, J.; Hammarling, S.; Demmel, J.; Bischof, C.; Bischof, C.; Sorensen, D. A10, LAPACK: A portable linear algebra library for high-performance computers; 1990; http://dx.doi.org/10.1109/SUPERC.1990.129995.
(177) Zimmerman, P. M.; Toulouse, J.; Zhang, Z.; Musgrave, C. B.; Umrigar, C. J. *J. Chem. Phys.* **2009**, *131*, 124103.
(178) Filippi, C.; Zaccheddu, M.; Buda, F. *J. Chem. Theor. Comput.* **2009**, *5*, 2074.
(179) Stevens, W.; Basch, H.; Krauss *J. Chem. Phys.* **1984**, *81*, 6026.
(180) Bachelet, G. B.; Ceperley, D. M.; Chiocchetti, M. G. B. *Phys. Rev. Lett.* **1989**, *62*, 2088.
(181) Burkatzki, M.; Filippi, C.; Dolg, M. *J. Chem. Phys.* **2008**, *129*, 164115.
(182) Burkatzki, M.; Filippi, C.; Dolg, M. *J. Chem. Phys.* **2007**, *126*, 234105.
(183) Casula, M. *Phys. Rev. B* **2006**, *74*, 161102.
(184) Casula, M.; Moroni, S.; Sorella, S.; Filippi, C. *J. Chem. Phys.* **2010**, *132*, 154113.
(185) Casula, M.; Filippi, C.; Sorella, S. *Phys. Rev. Lett.* **2005**, *95*, 100201.
(186) Pollack, L.; Windus, T. L.; de Jong, W. A.; Dixon, D. A. *J. Phys. Chem. A* **2005**, *109*, 6934.
(187) Kussmann, J.; Ochsenfeld, C. *J. Chem. Phys.* **2008**, *128*, 134104.
(188) Ceperley, D. M. *J. Stat. Phys.* **1986**, *43*, 815.
(189) Williamson, A. J.; Hood, R. Q.; Grossman, J. C. *Phys. Rev. Lett.* **2001**, *87*, 246406.
(190) Alfè, D.; Gillan, M. J. *J. Phys. Cond. Mat* **2004**, *16*, L305.
(191) Foster, J. M.; Boys, S. F. *Rev. Mod. Phys.* **1960**, *32*, 305.
(192) Aspuru-Guzik, A.; Salomon-Ferrer, R.; Austin, B.; Lester, W. A., Jr. *J. Comput. Chem.* **2005**, *26*, 708.
(193) Reboredo, F. A.; Williamson, A. *J. Phys. Rev. B* **2005**, *71*, 121105.
(194) Liu, S. B.; Perez-Jorda, J.; Yang, W. *J. Chem. Phys.* **2000**, *112*, 1634.
(195) Austin, B.; Aspuru-Guzik, A.; Salomon-Ferrer, R.; Lester, Jr., W. In *Advances in Quantum Monte Carlo*; Anderson, J., Rothstein, S., Eds.; American Chemical Society: Washington, DC, 2006.
(196) Sun, Z.; Reynolds, P.; Owen, R.; Lester, W. A., Jr. *Theor. Chem. Acc.* **1989**, *75*, 353.
(197) Aspuru-Guzik, A.; Salomon-Ferrer, R.; Austin, B.; Perusquia-Flores, R.; Griffin, M.; Oliva, R.; Skinner, D.; Domin, D.; Lester, W., Jr. *J. Comput. Chem.* **2005**, *26*, 856.
(198) Austin, B. Enhancing the quantum Monte Carlo method for electronic properties of large molecules and excited states, Ph.D. thesis, U. C. Berkeley, Berkeley, CA, 2009.
(199) Weber, R.; Gothandaraman, A.; Hinde, R. J.; Peterson, G. D. *IEEE Trans. Parallel Dist. Syst.* **2011**, *22*, 58.
(200) Meredith, J. S.; Alvarez, G.; Maier, T. A.; Schulthess, T. C.; Vetter, J. S. *Parallel Comput.* **2009**, *35*, 151.
(201) Anderson, A. G.; Goddard, W. A., III; Schroeder, P. *Comput. Phys. Commun.* **2007**, *177*, 298.
(202) Gothandaraman, A.; Peterson, G. D.; Warren, G. L.; Hinde, R. J.; Harrison, R. J. *Parallel Comput.* **2008**, *34*, 278.
(203) Korth, M.; Luechow, A.; Grimme, S. *J. Phys. Chem. A* **2008**, *112*, 2104.
(204) Luchow, A., et al. *Amolqc.* **2002**
(205) Anderson, D. BOINC; http://boinc.berkeley.edu.
(206) Feldmann, M. T.; Cummings, J. C.; Kent, D. R.; Muller, R. P.; Goddard, W. A., III *J. Comput. Chem.* **2008**, *29*, 8.
(207) Nilsen, J. K. *Comput. Phys. Commun.* **2007**, *177*, 799.
(208) Aspuru-Guzik, A.; Salomon-Ferrer, R.; Austin, B.; Perusquia-Flores, R.; Griffin, M. A.; Oliva, R. A.; Skinner, D.; Domin, D.; Lester, W. A., Jr. *J. Comput. Chem.* **2005**, *26*, 856.
(209) Olivares-Amaya, R.; Salomón-Ferrer, R.; Lester, W. A., Jr.; Amador-Bedolla, C. *Comput. Sci. Eng.* **2009**, *11*, 41.
(210) Wagner, L. K.; Bajdich, M.; Mitas, L. *J. Comput. Phys.* **2009**, *228*, 3390.
(211) Gillan, M. J.; Towler, M. G.; Alfe, D. *Psi-k Highlight of the Month*; 2011.
(212) http://www.mcc.uiuc.edu/qmc/qmcpack/index.html.
(213) http://pages.physics.cornell.edu/~cyrus/champ.html.
(214) Fisher, D. R.; Kent, D. R.; Feldmann, M. T.; Goddard, W. A., III *J. Comput. Chem.* **2008**, *29*, 2335.
(215) Nukala, P. K. V. V; Kent, P. R. C. J. *Chem. Phys.* **2009**, *130*, 204105.
(216) Clark, B. K.; Morales, M. A.; McMinis, J.; Kim, J.; Scuseria, G. E. arXiv:1106.2456v1 [cond−mat.mtrl−sci].
(217) Trail, J. R.; Maezono, R. *J. Chem. Phys.* **2010**, *133*, 174120.
(218) Hongo, K.; Maezono, R.; Miura, K. *J. Comput. Chem.* **2010**, *31*, 2186.
(219) Luan, T.; Curotto, E.; Mella, M. *J. Chem. Phys.* **2008**, *128*, 164102.
(220) Ramilowski, J. A.; Farrelly, D. *Phys. Chem. Chem. Phys.* **2010**, *12*, 12450.
(221) Toulouse, J.; Umrigar, C. J. *J. Chem. Phys.* **2008**, *128*, 174101.
(222) Luechow, A.; Petz, R.; Scott, T. C. *J. Chem. Phys.* **2007**, *126*, 144110.
(223) Scott, T. C.; Luechow, A.; Bressanini, D.; Morgan, J. D., III *Phys. Rev. A* **2007**, *75*, 060101.

(224) Vrbik, J.; DePasquale, M. F.; Rothstein, S. M. *J. Chem. Phys.* **1988**, *88*, 3784.
(225) Barnett, R. N.; Reynolds, P. J.; Lester, W. A., Jr. *J. Chem. Phys.* **1992**, *96*, 2141.
(226) Vrbik, J.; Legare, D. A.; Rothstein, S. M. *J. Chem. Phys.* **1990**, *92*, 1221.
(227) Vrbik, J.; Rothstein, S. M. *J. Chem. Phys.* **1992**, *96*, 2071.
(228) Vrbik, J.; Depasquale, M.; Rothstein, S. M. *J. Chem. Phys.* **1988**, *88*, 3784.
(229) Assaraf, R.; Caffarel, M. *J. Chem. Phys.* **2000**, *113*, 4028.
(230) Vrbik, J. *Int. J. Quantum Chem.* **2008**, *108*, 493.
(231) Gaudoin, R.; Pitarke, J. M. *Phys. Rev. Lett.* **2007**, *99*, 126406.
(232) Assaraf, R.; Caffarel, M. *J. Chem. Phys.* **2003**, *119*, 10536.
(233) Toulouse, J.; Assaraf, R.; Umrigar, C. J. *J. Chem. Phys.* **2007**, *126*, 244112.
(234) Per, M. C.; Russo, S. P.; Snook, I. K. *J. Chem. Phys.* **2008**, *128*, 114106.
(235) Lee, M. W.; Levchenko, S. V.; Rappe, A. M. *Mol. Phys.* **2007**, *105*, 2493.
(236) Sorella, S.; Capriotti, L. *J. Chem. Phys.* **2010**, *133*, 234111.
(237) Wagner, L. K.; Grossman, J. C. *Phys. Rev. Lett.* **2010**, *104*, 210201.
(238) Badinski, A.; Trail, J. R.; Needs, R. J. *J. Chem. Phys.* **2008**, *129*, 224101.
(239) Badinski, A.; Needs, R. *J. Phys. Rev. B* **2008**, *78*, 035134.
(240) Badinski, A.; Haynes, P. D.; Needs, R. *J. Phys. Rev. B* **2008**, *77*, 085111.
(241) Badinski, A.; Needs, R. *J. Phys. Rev. E* **2007**, *76*, 036707.
(242) Coles, B.; Vrbik, P.; Giacometti, R. D.; Rothstein, S. M. *J. Phys. Chem. A* **2008**, *112*, 2012.
(243) Purwanto, W.; Al-Saidi, W. A.; Krakauer, H.; Zhang, S. *J. Chem. Phys.* **2008**, *128*, 114309.
(244) Maldonado, P.; Sarsa, A.; Buendía, E.; Gálvez, F. J. *J. Chem. Phys.* **2010**, *133*, 064102.
(245) Brown, M. D.; Trail, J. R.; Rios, P. L.; Needs, R. J. *J. Chem. Phys.* **2007**, *126*, 224110.
(246) Drummond, N.; Rios, P.; Ma, A.; Trail, J.; Spink, G.; Towler, M.; Needs, R. *J. Chem. Phys.* **2006**, *124*, 224104.
(247) Sarsa, A.; Buendia, E.; Galvez, F. J.; Maldonado, P. *J. Phys. Chem. A* **2008**, *112*, 2074.
(248) Al-Saidi, W. A. *J. Chem. Phys.* **2008**, *129*, 064316.
(249) Caffarel, M.; Daudey, J.; Heully, J.; Ramirez-Solis, A. *J. Chem. Phys.* **2005**, *123*, 094102.
(250) Aissing, G. *Phys. Rev. A* **1991**, *44*, R2765.
(251) Nakatsuka, Y.; Nakajima, T.; Nakata, M.; Hirao, K. *J. Chem. Phys.* **2010**, *132*, 054102.
(252) Nakatsuka, Y.; Nakajima, T.; Hirao, K. *J. Chem. Phys.* **2010**, *132*, 174108.
(253) Ma, A.; Towler, M.; Drummond, N.; Needs, R. *J. Chem. Phys.* **2005**, *122*, 224322.
(254) Harkless, J. A. W.; Irikura, K. K. *Int. J. Quantum Chem.* **2006**, *106*, 2373.
(255) Galek, P. T. A.; Handy, N. C.; Lester, W. A., Jr. *Mol. Phys.* **2006**, *104*, 3069.
(256) Al-Saidi, W. A.; Zhang, S.; Krakauer, H. *J. Chem. Phys.* **2007**, *127*, 144101.
(257) Caffarel, M.; Hernandez-Lamoneda, R.; Scemama, A.; Ramirez-Solis, A. *Phys. Rev. Lett.* **2007**, *99*, 153001.
(258) Harkless, J. A. W.; Francisco, J. S. *J. Phys. Chem. A* **2008**, *112*, 2088.
(259) Berner, R.; Luechow, A. *J. Phys. Chem. A* **2010**, *114*, 13222.
(260) Wang, J.; Domin, D.; Austin, B.; Zubarev, D. Y.; McClean, J.; Frenklach, M.; Cui, T.; Lester, W. A., Jr. *J. Phys. Chem. A* **2010**, *114*, 9832.
(261) Kanai, Y.; Takeuchi, N. *J. Chem. Phys.* **2009**, *131*, 214708.
(262) Kita, Y.; Maezono, R.; Tachikawa, M.; Towler, M.; Needs, R. J. *J. Chem. Phys.* **2009**, *131*, 134310.
(263) Bande, A.; Luechow, A. *Phys. Chem. Chem. Phys.* **2008**, *10*, 3371.
(264) Koseki, J.; Maezono, R.; Tachikawa, M.; Towler, M. D.; Needs, R. J. *J. Chem. Phys.* **2008**, *129*, 085103.
(265) Trail, J. R.; Needs, R. J. *J. Chem. Phys.* **2005**, *122*, 174109.
(266) Nemec, N.; Towler, M. D.; Needs, R. J. *J. Chem. Phys.* **2010**, *132*, 034111.
(267) Anderson, J. B.; Traynor, C. A.; Boghosian, B. M. *J. Chem. Phys.* **1993**, *99*, 345.
(268) Mella, M.; Anderson, J. *J. Chem. Phys.* **2003**, *119*, 8225.
(269) Springall, R.; Per, M. C.; Russo, S. P.; Snook, I. K. *J. Chem. Phys.* **2008**, *128*, 114308.
(270) Wu, X.; Hu, X.; Dai, Y.; Du, C.; Chu, S.; Hu, L.; Deng, J.; Feng, Y. *J. Chem. Phys.* **2010**, *132*, 204304.
(271) Benedek, N. A.; Snook, I. K.; Towler, M. D.; Needs, R. J. *J. Chem. Phys.* **2006**, *125*, 104302.
(272) Gurtubay, I. G.; Needs, R. J. *J. Chem. Phys.* **2007**, *127*, 124306.
(273) Sorella, S.; Casula, M.; Rocca, D. *J. Chem. Phys.* **2007**, *127*, 014105.
(274) Beaudet, T. D.; Casula, M.; Kim, J.; Sorella, S.; Martin, R. M. *J. Chem. Phys.* **2008**, *129*, 164711.
(275) Ma, J.; Alfe, D.; Michaelides, A.; Wang, E. *J. Chem. Phys.* **2009**, *130*, 154303.
(276) Kanai, Y.; Grossman, J. C. *Phys. Rev. A* **2009**, *80*, 032504.
(277) Wu, Z.; Allendorf, M. D.; Grossman, J. C. *J. Am. Chem. Soc.* **2009**, *131*, 13918.
(278) Lawson, J. W.; Bauschlicher, C. W., Jr.; Toulouse, J.; Filippi, C.; Umrigar, C. *J. Chem. Phys. Lett.* **2008**, *466*, 170.
(279) Hongo, K.; Watson, M. A.; Sanchez-Carrera, R. S.; Iitaka, T.; Aspuru-Guzik, A. *J. Phys. Chem. Lett.* **2010**, *1*, 1789.
(280) Drummond, N. D.; Needs, R. J. *Phys. Rev. Lett.* **2007**, *99*, 166401.
(281) Spanu, L.; Sorella, S.; Galli, G. *Phys. Rev. Lett.* **2009**, *103*, 196401.
(282) Umari, P.; Marzari, N. *J. Chem. Phys.* **2009**, *131*, 094104.
(283) Santra, B.; Michaelides, A.; Fuchs, M.; Tkatchenko, A.; Filippi, C.; Scheffler, M. *J. Chem. Phys.* **2008**, *129*, 194111.
(284) Casellas, H.; Massera, C.; Buda, F.; Gamez, P.; Reedijk, J. *New J. Chem.* **2006**, *30*, 1561.
(285) Zaccheddu, M.; Filippi, C.; Buda, F. *J. Phys. Chem. A* **2008**, *112*, 1627; PMID: 18211047.
(286) Amovilli, C.; Filippi, C.; Floris, F. M. *J. Phys. Chem. B* **2006**, *110*, 26225.
(287) Amovilli, C.; Filippi, C.; Floris, F. M. *J. Chem. Phys.* **2008**, *129*, 244106.
(288) Flad, H. J.; Schautz, F.; Wang, Y.; Dolg, M. In *Recent Advances in Quantum Monte Carlo Methods, Part II*; Rothstein, S. M., Lester, W. A., Jr., Tanaka, S., Eds.; World Scientific: Singapore, 2002.
(289) Grossman, J.; Mitas, L. *Phys. Rev. Lett.* **2005**, *94*, 056403.
(290) Cho, H. M.; Lester, W. A., Jr. *J. Phys. Chem. Lett.* **2010**, *1*, 3376.
(291) Maezono, R.; Watanabe, H.; Tanaka, S.; Towler, M. D.; Needs, R. J. *J. Phys. Soc. Jpn.* **2007**, *76*, 064301.
(292) Attaccalite, C.; Sorella, S. *Phys. Rev. Lett.* **2008**, *100*, 114501.
(293) Miura, S. *Chem. Phys. Lett.* **2009**, *482*, 165–170.
(294) Oblinsky, D. G.; Yuen, W. K.; Rothstein, S. M. *J. Mol. Struct.* **2010**, *961*, 29.
(295) Alexander, S. A.; Coldwell, R. L. *Int. J. Quantum Chem.* **2009**, *109*, 385.
(296) Hakansson, P.; Mella, M. *J. Chem. Phys.* **2008**, *129*, 124101.
(297) Per, M. C.; Russo, S. P.; Snook, I. K. *J. Chem. Phys.* **2009**, *130*, 134103.
(298) Amovilli, C.; March, N. *J. Phys. A* **2006**, *39*, 7349.
(299) Pauzat, F.; Pilme, J.; Toulouse, J.; Ellinger, Y. *J. Chem. Phys.* **2010**, *133*, 054301.
(300) Grimes, R. M.; Hammond, B. L.; Reynolds, P. J.; Lester, W. A., Jr. *J. Chem. Phys.* **1986**, *85*, 4749.
(301) Schautz, F.; Filippi, C. *J. Chem. Phys.* **2004**, *120*, 10931.
(302) Schautz, F.; Buda, F.; Filippi, C. *J. Chem. Phys.* **2004**, *121*, 5836.
(303) Li, Y.; Vrbik, J.; Rothstein, S. M. *Chem. Phys. Lett.* **2007**, *445*, 345.
(304) Alexander, S.; Coldwell, R. *J. Chem. Phys.* **2006**, *124*, 054104.

(305) Alexander, S. A.; Coldwell, R. L. *Int. J. Quantum Chem.* **2008**, *108*, 2813.
(306) Matxain, J. M.; Rezabal, E.; Lopez, X.; Ugalde, J. M.; Gagliardi, L. *J. Chem. Phys.* **2008**, *128*, 194315.
(307) Fayton, F. A., Jr.; Gibson, A. A.; Harkless, J. A. W. *Int. J. Quantum Chem.* **2009**, *109*, 43.
(308) Purwanto, W.; Zhang, S.; Krakauer, H. *J. Chem. Phys.* **2009**, *130*, 094107.
(309) Zimmerman, P. M.; Toulouse, J.; Zhang, Z.; Musgrave, C. B.; Umrigar, C. J. *J. Chem. Phys.* **2009**, *131*, 124103.
(310) Valsson, O.; Filippi, C. *J. Chem. Theor. Comput.* **2010**, *6*, 1275.
(311) Bouabca, T.; Ben Amor, N.; Maynau, D.; Caffarel, M. *J. Chem. Phys.* **2009**, *130*, 114107.
(312) Dubecký, M.; Derian, R.; Mitas, L.; Štich, I. *J. Chem. Phys.* **2010**, *133*, 244301.
(313) Send, R.; Valsson, O.; Filippi, C. *J. Chem. Theor. Comput.* **2011**, *7*, 444.
(314) Scemama, A.; Chaquin, P.; Caffarel, M. *J. Chem. Phys.* **2004**, *121*, 1725.
(315) Scemama, A.; Caffarel, M.; Savin, A. *J. Comput. Chem.* **2007**, *28*, 442.
(316) Amador-Bedolla, C.; Salomon-Ferrer, R.; Lester, W. A., Jr.; Vazquez-Martinez, J. A.; Aspuru-Guzik, A. *J. Chem. Phys.* **2007**, *126*, 204308.
(317) Oyamada, T.; Hongo, K.; Kawazoe, Y.; Yasuhara, H. *J. Chem. Phys.* **2006**, *125*, 014101.
(318) Hongo, K.; Maezono, R.; Kawazoe, Y.; Yasuhara, H.; Towler, M.; Needs, R. *J. Chem. Phys.* **2004**, *121*, 7144.
(319) Mueller, C.; Flad, H.-J.; Kohout, M.; Reinhold, J. *Theor. Chem. Acc.* **2007**, *117*, 41.
(320) Hsing, C. R.; Chou, M. Y.; Lee, T. K. *Phys. Rev. A* **2006**, *74*, 032507.
(321) Hongo, K.; Kawazoe, Y.; Yasuhara, H. *Int. J. Quantum Chem.* **2007**, *107*, 1459.
(322) Luo, H.; Hackbusch, W.; Flad, H.-J. *Mol. Phys.* **2010**, *108*, 425.